BROKEN NEURAL SCALING LAWS

Anonymous authors
Paper under double-blind review

ABSTRACT

We present a smoothly broken power law functional form that accurately models and extrapolates the scaling behaviors of deep neural networks (i.e. how the evaluation metric of interest varies as the amount of compute used for training, number of model parameters, training dataset size, or upstream performance varies) for various architectures and for various tasks within a large and diverse set of upstream and downstream tasks, in zero-shot, prompted, and finetuned settings. This set includes large-scale vision, language, audio, video, diffusion generative modeling, multimodal learning, contrastive learning, AI alignment, robotics, arithmetic, unsupervised/self-supervised learning, and reinforcement learning (single agent and multi-agent). When compared to other functional forms for neural scaling behavior, this functional form yields extrapolations of scaling behavior that are considerably more accurate on this set. Moreover, this functional form accurately models and extrapolates scaling behavior that other functional forms are incapable of expressing such as the non-monotonic transitions present in the scaling behavior of phenomena such as double descent and the delayed, sharp inflection points present in the scaling behavior of tasks such as arithmetic. Lastly, we use this functional form to glean insights about the limit of the predictability of scaling behavior.

1 INTRODUCTION

The amount of compute used for training, number of model parameters, and training dataset size of the most capable artificial neural networks keeps increasing and will probably keep rapidly increasing for the foreseeable future. However, no organization currently has direct access to these larger resources of the future; and it has been empirically verified many times that methods which perform best at smaller scales often are no longer the best performing methods at larger scales (e.g., one of such examples can be seen in Figure 2 (right) of Tolstikhin et al. (2021)). To work on, identify, and steer the methods that are most probable to stand the test-of-time as these larger resources come online, one needs a way to predict how all relevant performance evaluation metrics of artificial neural networks vary in all relevant settings as scale increases.

Neural scaling laws (Cortes et al., 1994; Hestness et al., 2017; Rosenfeld et al., 2019; Kaplan et al., 2020; Zhai et al., 2021; Abnar et al., 2021; Alabdulmohsin et al., 2022; Brown et al., 2020) aim to predict the behavior of large-scale models from smaller, cheaper experiments, allowing to focus on the best-scaling architectures, algorithms, datasets, and so on. The upstream/in-distribution test loss typically (but not always!) falls off as a power law with increasing data, model size and compute. However, the downstream/out-of-distribution performance, and other evaluation metrics of interest (even upstream/in-distribution evaluation metrics) are often less predictable, sometimes exhibiting inflection points (on a linear-linear plot) and non-monotonic behaviors. Discovering *universal scaling laws* that accurately model a wide range of potentially unexpected behaviors is clearly important not only for identifying that which scales best, but also for AI safety, as predicting the emergence of novel capabilities at scale could prove crucial to responsibly developing and deploying increasingly advanced AI systems. The functional forms of scaling laws evaluated in previous work are not up to this challenge.

One salient defect is that they can only represent monotonic functions. They thus fail to model the striking phenomena of double-descent (Nakkiran et al., 2021), where increased scale temporarily decreases test performance before ultimately leading to further improvements. Many also lack the expressive power to model inflection points (on a linear-linear plot), which can be observed empirically for many downstream tasks, and even some upstream tasks, such as our N-digit arithmetic task, or the modular arithmetic task introduced by Power et al. (2022) in their work on "grokking".

To overcome the above limitations, we present *broken neural scaling laws (BNSL)* - a functional form that generalizes power laws (linear in log-log plot) to "smoothly broken" power laws, i.e.

a smoothly connected piecewise (approximately) linear function in a log-log plot. An extensive empirical evaluation demonstrates that BNSL accurately model and extrapolate the scaling behaviors for various tasks within a large and diverse set of upstream and downstream tasks, in zero-shot, prompted, and fine-tuned settings. This set includes large-scale vision, language, audio, video, diffusion generative modeling, multimodal learning, contrastive learning, AI alignment, robotics, arithmetic, unsupervised/self-supervised learning, and reinforcement learning (single agent and multi-agent). When compared to other functional forms for neural scaling behavior, this functional form yields extrapolations of scaling behavior that are considerably more accurate on this set. It captures well the non-monotonic transitions present in the scaling behavior of phenomena such as double descent and the delayed, sharp inflection points present in the scaling behavior of tasks such as arithmetic.

2 THE FUNCTIONAL FORM OF BROKEN NEURAL SCALING LAWS

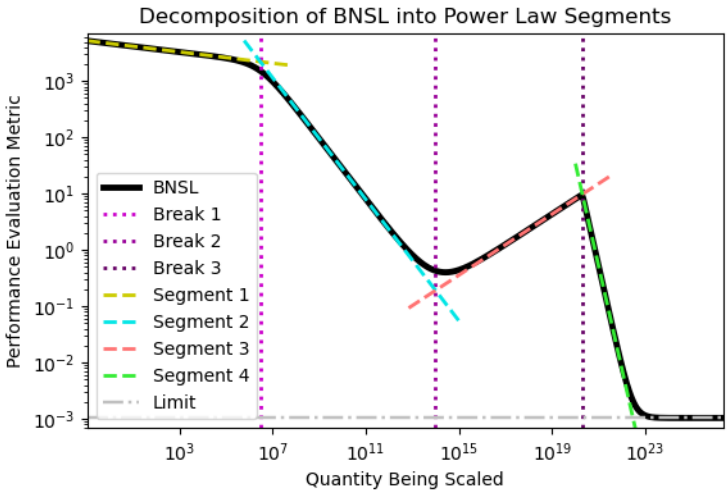

Figure 1: A Broken Neural Scaling Law (BNSL) (dark black solid line) with 3 breaks (where purple dotted lines intersect with dark black solid line) decomposed into the individual power laws (dashed lines that are yellow, blue, red, and green) that it is composed of overlaid on top of it. The 1st and 2nd break are very smooth; the 3rd break is very sharp. See Section 2 for more details.

The general functional form of a broken neural scaling law (BNSL) is given as follows:

$$y = a + \left(bx^{-c_0}\right) \prod_{i=1}^{n} \left(1 + \left(\frac{x}{d_i}\right)^{1/f_i}\right)^{-c_i * f_i}, \tag{1}$$

where y represents the performance evaluation metric (e.g. prediction error, cross entropy, BLEU score percentage, reward, Elo rating, or FID score) (**downstream or upstream**) and x represents a quantity that is being scaled (e.g. number of model parameters, amount of compute used for training, training dataset size, or upstream performance). The remaining parameters $a, b, c_0, c_1...c_n, d_1...d_n, f_1...f_n$ are unknown constants that must be estimated by fitting the above functional form to the (x, y) data points. (In our experiments, SciPy curve-fitting library (Virtanen et al., 2020) was used.)

The constants in equation 1 are interpreted as follows. Constant n represents the number of (smooth) "breaks" (i.e. transitions) between $n + 1$ consecutive approximately linear (on a log-log plot) segments, for a total of $n + 1$ approximately linear segments (on a log-log plot). Constant a represents the limit as to how far the value of y (performance evaluation metric) can be reduced (or maximized) even if x (the quantity being scaled) goes to infinity. Constant b represents the offset of functional form on a log-log plot (analogous to the intercept b in $y = mx + b$ on a linear-linear plot). Constant c_0 represents the slope of the first approximately linear region on a log-log plot. Constant c_i represents the difference in slope of the (i)th approximately linear region and $(i + 1)$th approximately linear region on a log-log plot. Constant d_i represents where on the x-axis the break between the

(i)th and the $(i+1)$th approximately linear region (on a log-log plot) occurs. Constant f_i represents the sharpness of break between the (i)th and the $(i+1)$th approximately linear region on a log-log plot; smaller (nonnegative) values of f_i yield a sharper break and intervals (before and after the (i)th break) that are more linear on a log-log plot; larger values of f_i yield a smoother break and intervals (before and after the (i)th break) that are less linear on a log-log plot.

For mathematical analysis and explanation of why Equation 1 is smoothly piece-wise (approximately) linear function on a log-log plot, see Appendix A.2. For mathematical decomposition of Equation 1 into the power law segments it is composed of (e.g. as in Figure 1), see Appendix A.3.

Note that, while an intuition for using such smoothly connected approximately piece-wise linear (in log-log plot) function was that, with enough segments, it could fit well any smooth univariate scaling function, it remained unclear whether BNSL would also *extrapolate* well; as we demonstrate below, it does extrapolate quite accurately in our experiments. Additionally, we find that the number of breaks needed to accurately model an entire scaling behavior is often quite small.

3 Empirical Results: Fits and Extrapolations of Functional Forms

We now show the fits and extrapolations of various functional forms. In all plots here and onward and in the appendix, **black points are points used for fitting a functional form, green points are the held-out points used for evaluating extrapolation of a functional form fit to the black points, and a red line is the BNSL that has been fit to black points**. Please refer to Appendix Section A.7 for further experimental details on fitting BNSL.

Except when stated otherwise, each plot contains a single break of a BNSL fit to black points that are smaller (along the x-axis) than the green points.

In the tables and elsewhere, M1 refers to functional form $y = ax^b$, M2 refers to functional form $y = ax^b + c$, M3 refers to functional form $y = a(x^{-1} + d)^{-b} + c$, M4 refers to functional form $(y - \epsilon_\infty)/((\epsilon_0 - y)^a) = bx^c$. For a detailed history and related work concerning these functional forms, see section A.1. See section A.8 for a mathematical explanation of the theoretical limitations of previously proposed scaling laws.

All the extrapolation evaluations reported in the tables are reported in terms of root mean squared log error (RMSLE) ± root standard log error. See Appendix A.4 for definition of RMSLE and Appendix A.5 for definition of root standard log error.

See appendix for plots of extrapolation results on large-scale vision, language, audio, video, diffusion generative modeling, multimodal learning, contrastive learning, AI alignment, robotics, arithmetic, unsupervised/self-supervised learning, and reinforcement learning (single agent and multi-agent). See section A.12 for example of BNSL modeling and extrapolating a non-monotonic scaling behavior with 2 breaks.

Domain	M1 ↑	M2 ↑	M3 ↑	M4 ↑	BNSL ↑
Downstream Image Classification	2.78%	4.17%	9.72%	13.89%	**69.44%**
Language	10%	5%	25%	0%	**60%**

Table 1: Percentage of tasks by domain where each functional form is the best for extrapolation of scaling behavior. Numbers for M1, M2, M3, and M4 were obtained via correspondence with authors of Alabdulmohsin et al. (2022). See Sections A.9 and A.10 for more details.

3.1 Inflection Points

We show that BNSL is capable of modeling and extrapolating the scaling behavior of tasks that have an inflection point on a linear-linear plot such as the task of arithmetic (4-digit addition). Here we model and extrapolate the scaling behavior of a transformer model (Vaswani et al. (2017)) with respect to the training dataset size on the 4-digit addition task. Various other functional forms are mathematically incapable of expressing inflection points on a linear-linear plot (as shown in Section A.8) and as a result, are mathematically incapable of expressing and modeling inflection points (on a linear-linear plot) that are present in the scaling behavior of 4-digit addition. In Figure 2 left, we show that BNSL expresses and accurately models the inflection point present in the scaling behavior of 4-digit addition and as a result accurately extrapolates the scaling behavior of 4 digit addition. For further details about the hyperparameters please refer to the Appendix Section A.6.

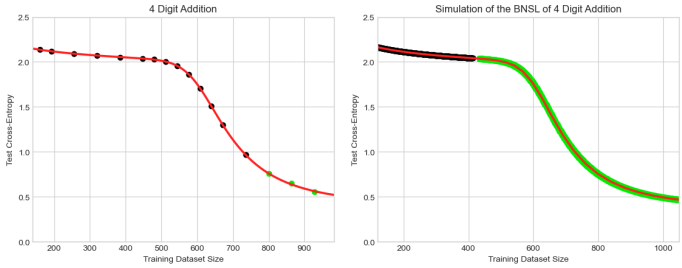

Figure 2: Extrapolation of BNSL on 4 Digit Addition. Note that these plots are linear-linear. Each point in the left plot is the mean of greater than 1000 seeds at that dataset size. In the left plot, each point is gathered from a model trained to do the task of 4 digit addition. In the right plot, each point is gathered from a noiseless simulation of the BNSL of the task of 4 digit addition. See Sections 3.1, A.6, 4, for more details.

4 The Limit of the Predictability of Scaling Behavior

We use BNSL to glean insights about the limit of the predictability of scaling behavior. Recent papers (Ganguli et al., 2022; Wei et al., 2022) have advertised many tasks as having "unpredictable" "emergent" "phase transition/change" scaling behavior, the most famous of which is the task of arithmetic. In the previous section and in Figure 2 left, we successfully predicted (i.e. extrapolated) the scaling behavior of 4-digit addition (arithmetic). However, we are only able to accurately extrapolate the scaling behavior if given some points from training runs with a training dataset size of at least 720, and the break in which the scaling behavior of 4-digit addition transitions from one power law to another steeper power-law happens at around training dataset size of 415.

Ideally, one would like to be able to extrapolate the entire scaling behavior by fitting only points from before the break. In Figure 2 right, we use a noiseless simulation of the BNSL of 4-digit addition to show what would happen if one had infinitely many training runs / seeds to average out all the noisy deviation between runs such that one could recover (i.e. learn via a curve-fitting library such as SciPy (Virtanen et al., 2020)) the learned constant of the BNSL as well as possible. When using this noiseless simulation, we find that we are only able to accurately extrapolate the scaling behavior if given some points from training runs with a training dataset size of at least 415, which is very close to the break.

This has a few implications:

1) When the scaling behavior exhibits greater than zero breaks that are sufficiently sharp, there is a limit as to how small the maximum (along the x-axis) of the points used for fitting can be if one wants to perfectly extrapolate the scaling behavior, even if one has infinitely many seeds / training runs. 2) If an additional break of sufficient sharpness happens at a scale that is sufficiently larger than the maximum (along the x-axis) of the points used for fitting, there does not (currently) exist a way to extrapolate the scaling behavior after that additional break. 3) If a break of sufficient sharpness happens at a scale sufficiently smaller than the maximum (along the x-axis) of the points used for fitting, points smaller (along the x-axis) than that break are often useless for improving extrapolation.

5 Conclusions

Summary. We have presented a smoothly broken power law functional form that accurately models and extrapolates the scaling behaviors of artificial neural networks for various architectures and for various tasks from a very large and diverse set of upstream and downstream tasks. This set includes large-scale vision, language, audio, video, diffusion generative modeling, multimodal learning, contrastive learning, AI alignment, robotics, arithmetic, unsupervised/self-supervised learning, and reinforcement learning (single agent and multi-agent). When compared to other functional forms for neural scaling behavior, this functional form yields extrapolations of scaling behavior that are considerably more accurate on this set. Additionally, this functional form accurately models and extrapolates scaling behavior that other functional forms are incapable of expressing such as the non-monotonic transitions present in the scaling behavior of phenomena such as double descent and the delayed, sharp inflection points present in the scaling behavior of tasks such as arithmetic. Finally, we used this functional form to obtain insights about the limit of the predictability of scaling behavior.

REFERENCES

Direct detection of a break in the teraelectronvolt cosmic-ray spectrum of electrons and positrons. *Nature*, 552(7683):63–66, nov 2017. doi: 10.1038/nature24475. URL https://doi.org/10.1038%2Fnature24475.

Samira Abnar, Mostafa Dehghani, Behnam Neyshabur, and Hanie Sedghi. Exploring the limits of large scale pre-training, 2021.

Ibrahim Mansour I Alabdulmohsin, Behnam Neyshabur, and Xiaohua Zhai. Revisiting neural scaling laws in language and vision. In *NeurIPS 2022*, 2022. URL https://arxiv.org/abs/2209.06640.

Yuntao Bai, Andy Jones, Kamal Ndousse, Amanda Askell, Anna Chen, Nova DasSarma, Dawn Drain, Stanislav Fort, Deep Ganguli, Tom Henighan, et al. Training a helpful and harmless assistant with reinforcement learning from human feedback. *arXiv preprint arXiv:2204.05862*, 2022.

Tom Brown, Benjamin Mann, Nick Ryder, Melanie Subbiah, Jared D Kaplan, Prafulla Dhariwal, Arvind Neelakantan, Pranav Shyam, Girish Sastry, Amanda Askell, et al. Language models are few-shot learners. *Advances in neural information processing systems*, 33:1877–1901, 2020.

Karl Cobbe, Chris Hesse, Jacob Hilton, and John Schulman. Leveraging procedural generation to benchmark reinforcement learning. In *International conference on machine learning*, pp. 2048–2056. PMLR, 2020.

Corinna Cortes, Lawrence D Jackel, Sara A Solla, Vladimir Vapnik, and John S Denker. Learning curves: Asymptotic values and rate of convergence. In *Advances in Neural Information Processing Systems*, pp. 327–334, 1994.

Jia Deng, Wei Dong, Richard Socher, Li-Jia Li, Kai Li, and Li Fei-Fei. Imagenet: A large-scale hierarchical image database. In *2009 IEEE conference on computer vision and pattern recognition*, pp. 248–255. Ieee, 2009.

Alexey Dosovitskiy, Lucas Beyer, Alexander Kolesnikov, Dirk Weissenborn, Xiaohua Zhai, Thomas Unterthiner, Mostafa Dehghani, Matthias Minderer, Georg Heigold, Sylvain Gelly, et al. An image is worth 16x16 words: Transformers for image recognition at scale. *arXiv preprint arXiv:2010.11929*, 2020.

Li Fei-Fei, Rob Fergus, and Pietro Perona. Learning generative visual models from few training examples: An incremental bayesian approach tested on 101 object categories. In *2004 conference on computer vision and pattern recognition workshop*, pp. 178–178. IEEE, 2004.

Deep Ganguli, Danny Hernandez, Liane Lovitt, Amanda Askell, Yuntao Bai, Anna Chen, Tom Conerly, Nova Dassarma, Dawn Drain, Nelson Elhage, et al. Predictability and surprise in large generative models. In *2022 ACM Conference on Fairness, Accountability, and Transparency*, pp. 1747–1764, 2022.

Tom Henighan, Jared Kaplan, Mor Katz, Mark Chen, Christopher Hesse, Jacob Jackson, Heewoo Jun, Tom B. Brown, Prafulla Dhariwal, Scott Gray, Chris Hallacy, Benjamin Mann, Alec Radford, Aditya Ramesh, Nick Ryder, Daniel M. Ziegler, John Schulman, Dario Amodei, and Sam McCandlish. Scaling Laws for Autoregressive Generative Modeling. *arXiv e-prints*, art. arXiv:2010.14701, October 2020.

Danny Hernandez, Jared Kaplan, Tom Henighan, and Sam McCandlish. Scaling Laws for Transfer. *arXiv e-prints*, art. arXiv:2102.01293, February 2021.

Joel Hestness, Sharan Narang, Newsha Ardalani, Gregory Diamos, Heewoo Jun, Hassan Kianinejad, Md. Mostofa Ali Patwary, Yang Yang, and Yanqi Zhou. Deep Learning Scaling is Predictable, Empirically. *arXiv e-prints*, art. arXiv:1712.00409, December 2017.

J. D. Hunter. Matplotlib: A 2d graphics environment. *Computing in Science & Engineering*, 9(3): 90–95, 2007. doi: 10.1109/MCSE.2007.55.

Jared Kaplan, Sam McCandlish, Tom Henighan, Tom B. Brown, Benjamin Chess, Rewon Child, Scott Gray, Alec Radford, Jeffrey Wu, and Dario Amodei. Scaling Laws for Neural Language Models. *arXiv e-prints*, art. arXiv:2001.08361, January 2020.

Andrej Karpathy. mingpt. `https://github.com/karpathy/minGPT`, 2020.

Alexander Kolesnikov, Lucas Beyer, Xiaohua Zhai, Joan Puigcerver, Jessica Yung, Sylvain Gelly, and Neil Houlsby. Big transfer (bit): General visual representation learning. In *European conference on computer vision*, pp. 491–507. Springer, 2020.

Alex Krizhevsky, Geoffrey Hinton, et al. Learning multiple layers of features from tiny images. 2009.

Preetum Nakkiran, Gal Kaplun, Yamini Bansal, Tristan Yang, Boaz Barak, and Ilya Sutskever. Deep double descent: Where bigger models and more data hurt. *Journal of Statistical Mechanics: Theory and Experiment*, 2021(12):124003, 2021.

Oren Neumann and Claudius Gros. Scaling laws for a multi-agent reinforcement learning model. *arXiv preprint arXiv:2210.00849*, 2022.

Alexander Quinn Nichol and Prafulla Dhariwal. Improved denoising diffusion probabilistic models. In *International Conference on Machine Learning*, pp. 8162–8171. PMLR, 2021.

Alethea Power, Yuri Burda, Harri Edwards, Igor Babuschkin, and Vedant Misra. Grokking: Generalization beyond overfitting on small algorithmic datasets. *arXiv preprint arXiv:2201.02177*, 2022.

Alec Radford, Jong Wook Kim, Chris Hallacy, Aditya Ramesh, Gabriel Goh, Sandhini Agarwal, Girish Sastry, Amanda Askell, Pamela Mishkin, Jack Clark, et al. Learning transferable visual models from natural language supervision. In *International Conference on Machine Learning*, pp. 8748–8763. PMLR, 2021.

Alec Radford, Jong Wook Kim, Tao Xu, Greg Brockman, Christine McLeavey, and Ilya Sutskever. Robust speech recognition via large-scale weak supervision. *arXiv preprint arXiv:2212.04356*, 2022.

Jonathan S. Rosenfeld, Amir Rosenfeld, Yonatan Belinkov, and Nir Shavit. A constructive prediction of the generalization error across scales. *CoRR*, abs/1909.12673, 2019. URL `http://arxiv.org/abs/1909.12673`.

John Schulman, Filip Wolski, Prafulla Dhariwal, Alec Radford, and Oleg Klimov. Proximal policy optimization algorithms. *arXiv preprint arXiv:1707.06347*, 2017.

Mohit Shridhar, Lucas Manuelli, and Dieter Fox. Cliport: What and where pathways for robotic manipulation. In *Proceedings of the 5th Conference on Robot Learning (CoRL)*, 2021.

Ben Sorscher, Robert Geirhos, Shashank Shekhar, Surya Ganguli, and Ari S. Morcos. Beyond neural scaling laws: beating power law scaling via data pruning, 2022. URL `https://arxiv.org/abs/2206.14486`.

Aarohi Srivastava, Abhinav Rastogi, Abhishek Rao, Abu Awal Md Shoeb, Abubakar Abid, Adam Fisch, Adam R Brown, Adam Santoro, Aditya Gupta, Adrià Garriga-Alonso, et al. Beyond the imitation game: Quantifying and extrapolating the capabilities of language models. *arXiv preprint arXiv:2206.04615*, 2022.

Chen Sun, Abhinav Shrivastava, Saurabh Singh, and Abhinav Gupta. Revisiting unreasonable effectiveness of data in deep learning era. In *Proceedings of the IEEE international conference on computer vision*, pp. 843–852, 2017.

Ilya O Tolstikhin, Neil Houlsby, Alexander Kolesnikov, Lucas Beyer, Xiaohua Zhai, Thomas Unterthiner, Jessica Yung, Andreas Steiner, Daniel Keysers, Jakob Uszkoreit, et al. Mlp-mixer: An all-mlp architecture for vision. *Advances in Neural Information Processing Systems*, 34:24261–24272, 2021.

Aaron Van Den Oord, Oriol Vinyals, et al. Neural discrete representation learning. *Advances in neural information processing systems*, 30, 2017.

Ashish Vaswani, Noam Shazeer, Niki Parmar, Jakob Uszkoreit, Llion Jones, Aidan N Gomez, Łukasz Kaiser, and Illia Polosukhin. Attention is all you need. *Advances in neural information processing systems*, 30, 2017.

Pauli Virtanen, Ralf Gommers, Travis E Oliphant, Matt Haberland, Tyler Reddy, David Cournapeau, Evgeni Burovski, Pearu Peterson, Warren Weckesser, Jonathan Bright, et al. Scipy 1.0: fundamental algorithms for scientific computing in python. *Nature methods*, 17(3):261–272, 2020.

Jason Wei, Yi Tay, Rishi Bommasani, Colin Raffel, Barret Zoph, Sebastian Borgeaud, Dani Yogatama, Maarten Bosma, Denny Zhou, Donald Metzler, et al. Emergent abilities of large language models. *arXiv preprint arXiv:2206.07682*, 2022.

Peter Welinder, Steve Branson, Takeshi Mita, Catherine Wah, Florian Schroff, Serge Belongie, and Pietro Perona. Caltech-ucsd birds 200. 2010.

Andy Zeng, Pete Florence, Jonathan Tompson, Stefan Welker, Jonathan Chien, Maria Attarian, Travis Armstrong, Ivan Krasin, Dan Duong, Vikas Sindhwani, et al. Transporter networks: Rearranging the visual world for robotic manipulation. In *Conference on Robot Learning*, pp. 726–747. PMLR, 2021.

Xiaohua Zhai, Alexander Kolesnikov, Neil Houlsby, and Lucas Beyer. Scaling vision transformers. *CoRR*, abs/2106.04560, 2021. URL `https://arxiv.org/abs/2106.04560`.

A APPENDIX

A.1 RELATED WORK

To the best of our knowledge, Cortes et al. (1994) was the first paper to model the scaling of multi-layer neural network's performance as a power law (also known as a scaling law) (plus a constant) of the form $y = ax^b + c$ in which x refers to training dataset size and y refers to test error; we refer to that functional form as M2. Hestness et al. (2017) showed that the functional form, M2, holds over many orders of magnitude. Rosenfeld et al. (2019) demonstrated that the same functional form, M2, applies when x refers to model size (number of parameters). Kaplan et al. (2020) brought "neural" scaling laws to the mainstream and demonstrated that the same functional form, M2, applies when x refers to the amount of compute used for training. Abnar et al. (2021) proposed to use the same functional form, M2, to relate downstream performance to upstream performance. Zhai et al. (2021) introduced the functional form $y = a(x + d)^b + c$, (referred to by us as M3) where d represents the scale at which the performance starts to improve beyond the random guess loss (a constant) and transitions to a power law scaling regime. Alabdulmohsin et al. (2022) proposed functional form $(y - \epsilon_\infty)/((\epsilon_0 - y)^a) = bx^c$, (referred to by us as M4) where ϵ_∞ is irreducible entropy of the data distribution and ϵ_0 is random guess performance, for relating scale to performance and released a scaling laws benchmark dataset that we use in our experiments.

Hernandez et al. (2021) described a smoothly broken power law functional form (consisting of 5 constants after reducing redundant variables) in equation 6.1 of their paper, when relating scale and downstream performance. While this functional form can be summed with an additional constant representing unimprovable performance to obtain a functional form that is mathematically equivalent to our BNSL with a single break, it is important to note that (i) Hernandez et al. (2021) describes this form only in the specific context, when exploring how fine-tuning combined with transfer learning scales as a function of the model size - thus, their functional form contains a break only with respect to number of model parameters but not with respect to other input quantities which we do explore such as dataset size, amount of compute, and upstream performance; (ii) Hernandez et al. (2021) mentioned this equation in passing and as a result did not try to fit or verify this functional form on any data; (iii) they arrived at it simply via combining the scaling law for transfer (that was the focus of their work) with a scaling law for pretraining data; (iv) they did not identify it as a smoothly broken power law, or note any qualitative advantages of this functional form; (v) they did not discuss the family of functional forms with multiple breaks.

Finally, we would like to mention that smoothly broken power law functional forms, equivalent to equation 1, are commonly used in the astrophysics literature (e.g. dam (2017)) as they happen to model well a variety of physical phenomena. This inspired us to investigate their applicability to a wide range of deep neural scaling phenomena as well.

A.2 Analysis and Explanation of why BNSL is smoothly connected piecewise (approximately) linear function on a log-log plot

Analysing Equation 1 reveals why BNSL is smoothly connected piecewise (approximately) linear function on a log-log plot. Considering y as a function of $z := \log(x)$, applying logarithms to both sides and setting $a = 0$ yields:

$$\log(y) = \log(b) - c_0 z - \sum_{i=1}^{n} c_i f_i \log\left(1 + \left(\frac{\exp(z)}{d_i}\right)^{1/f_i}\right). \tag{2}$$

We can now see the terms in the sum resemble the well-known $\mathrm{softplus}$ function: $\mathrm{softplus}(x) := \log(1 + exp(x))$, which smoothly interpolates between the constant 0 function and the identity. By plotting one such term for different values of c_i, d_i, f_i, it is easy to confirm that they influence the shape of the curve as described in Section 2.

A.3 Decomposition of Broken Neural Scaling Law into power law segments that it is composed of

We now show a way to decompose a BNSL (Equation 1) with 3 breaks into the power law segments that it is composed of. This decomposition is what we used to produce segments 1-4 overlaid in Figure 1 and is usable when values of f in Equation 1 are not too large. This decomposition pattern is straight-forward to extend to n breaks.

$segment_1 = b * (x)^{-(c_0)}$

$segment_2 = b * (d_1)^{-(c_0)} * (x\ /d_1)^{-(c_1+c_0)}$

$segment_3 = b * (d_1)^{-(c_0)} * (d_2/d_1)^{-(c_1+c_0)} * (x\ /d_2)^{-(c_2+c_1+c_0)}$

$segment_4 = b * (d_1)^{-(c_0)} * (d_2/d_1)^{-(c_1+c_0)} * (d_3/d_2)^{-(c_2+c_1+c_0)} * (x\ /d_3)^{-(c_3+c_2+c_1+c_0)}$

A.4 Definition of Root Mean Squared Log Error

$$Root_Mean_Squared_Log_Error = RMSLE = \sqrt{(\sum_{i=1}^{n}(log(y_i) - log(\hat{y}_i))^2)/n}$$

A.5 Definition of Root Standard Log Error

$$error = (log(y_i) - log(\hat{y}_i))^2)$$

$$\mu_{error} = \frac{1}{N}\sum_{i=1}^{N} error$$

$$\sigma_{error} = \sqrt{\frac{1}{N-1}\sum_{i=1}^{N}(error_i - \mu_{error})^2}$$

$$Root_Standard_Log_Error = \sqrt{\mu_{error} + \frac{\sigma_{error}}{\sqrt{len(\hat{y})}}} - \sqrt{\mu_{error}}$$

A.6 Experimental details of Section 3.1

We perform an extensive set of experiments to model and extrapolate the scaling behavior for the 4-digit arithmetic addition task with respect to the training dataset size. Our code is based on the minGPT implementation (Karpathy, 2020). We set the batch size equal to the training dataset size. We do not use dropout or a learning rate decay here. Each experiment was run on a single V100 GPU and each run took less than 2 hours. For our experiments we train the transformer model using the following set of hyperparameters:

D_{model}	128
D_{MLP}	512
Number of heads	2
Number of transformer blocks (i.e. layers)	1
Learning rate	0.0001
Weight Decay	0.1
Dropout Probability	0.0
Dataset sizes	144-1008
Vocab Size	10

Table 2: Hyperparameters for 4-digit addition task

A.7 Experimental details of fitting BNSL

We fit BNSL as follows: We first use scipy.optimize.brute to do a grid search of the values of the constants $(a, b, c_0, c_1...c_n, d_1...d_n, f_1...f_n)$ of BNSL that best minimize the mean squared log error (MSLE) between the real data and the output of BNSL. We then use the values obtained from the grid search as the initialization of the non-linear least squares algorithm of scipy.optimize.curve_fit. We then use the non-linear least squares algorithm of scipy.optimize.curve_fit to minimize the mean squared log error (MSLE) between the real data and the output of BNSL.

The version of MSLE we use for such optimization is the following numerically stable variant:

$$Numerically_Stable_MSLE = \sum_{i=1}^{n}((log(y_i + 1) - log(\hat{y}_i + 1))^2)/n$$

A.8 THEORETICAL LIMITATIONS OF PREVIOUSLY PROPOSED SCALING LAWS

Our use of BNSLs is inspired by the observation that scaling is not always well predicted by a simple power law; nor are many of the modifications which have been applied in previous works sufficient to capture the qualitative properties of empirical scaling curves. Here we show mathematically two qualitative defects of these functional forms:

1. They are strictly monotonic (first-order derivative does not change its sign) and thus unable to fit double descent phenomena.
2. They cannot express inflection points (second-order derivative does not change its sign), which are frequently observed empirically. An exception to this is M4, proposed by Alabdulmohsin et al. (2022).

Note that these functional forms *can* exhibit inflection points on the log-log axes which are commonly used for plotting scaling data (as it was observed in several prior works). However, for inflection points on a *linear-linear* plot, the extra expressiveness of broken neural scaling laws appears to be necessary (and sufficient). Figure 4 and Figure 2, provide examples of BNSLs producing non-monotonic behavior and inflection points, respectively, establishing the capacity of this functional form to model these phenomena that occur in real scaling behavior.

name	$f(x)$	$f'(x)$	$f''(x)$
M1	ax^b	abx^{b-1}	$ab(b-1)x^{b-2}$
M2	$ax^b + c$	abx^{b-1}	$ab(b-1)x^{b-2}$
M3	$a(x^{-1}+d)^{-b} + c$	$\frac{ab}{x(1+dx)(d+1/x)^b}$	$abx^{(b-2)}(1+dx)^{(-2-b)}(b-1-2dx)$

Table 3: Previously proposed functional forms M1, M2, M3 and their (first and second order) derivatives. See Equation 3 for M4.

M1, M2, M3 functional forms cannot model non-monotonic behavior or inflection points: First, recall that expressions of the form m^n can only take the value 0 if $m = 0$. We now examine the expressions for the first and second derivatives of M1, M2, M3, provided in Table 3, and observe that they are all continuous and do not have roots over the relevant ranges of their variables, i.e. $x > 0$ in general and $b < 0$ in the case of M3 (we require $x > 0$ because model size, dataset size, and compute are always non-negative). This implies that, for any valid settings of the parameters a, b, c, d, x, these functional forms are monotonic (as the first derivative never changes sign), and that they lack inflection points (since an inflection point must have $f''(x) = 0$).

M4 functional form cannot model non-monotonic behavior. The case of M4 is a bit different, since the relationship between y and x in this case is expressed as an inverse function, i.e.

$$x = g(y) = \left(\frac{y - \epsilon_\infty}{b(\epsilon_0 - y)^a}\right)^{1/c} \tag{3}$$

However, non-monotonicity of y as an inverse function $y = g^{-1}(x)$ is ruled out, since that would imply two different values of $x = g(y)$ can be obtained for the single value of y – this is impossible, since $f(y)$ maps each y deterministically to a single value of x. As a result, M4 cannot express non-monotonic functions.

M4 functional form can model inflection points. It is easy to see that if $y = g^{-1}(x)$ had an inflection point, then $x = g(y)$ would have it as well. This is because an inflection point is defined as a point x where $f(x)$ changes from concave to convex, which implies that $g(y)$ changes from convex to concave, since the inverse of a convex function is concave; the root(s) of $g''(y)$ are the point(s) at which this change occurs. Using Wolfram Alpha[1] and matplotlib (Hunter, 2007), we observe that M4 is able to express inflection points, e.g. $(a, b, c, \epsilon_0, \epsilon_\infty, x, y) = (1, 1, -2, 3/4, 1/4, 1/\sqrt{3}, 5/8)$, or $(a, b, c, \epsilon_0, \epsilon_\infty, x, y) = (2, 1, -3, 2/3, 1/3, (-5/6 + \sqrt{3}/2)^{1/3}, 1/\sqrt{3})$.

[1] https://www.wolframalpha.com/

A.9 VISION

Using the scaling laws benchmark of Alabdulmohsin et al. (2022), we evaluate how well various functional forms extrapolate performance on vision tasks as training dataset size increases. In this large-scale vision subset of the benchmark, the tasks that are evaluated are error rate on each of various few-shot downstream image classification (IC) tasks; the downstream tasks are: Birds 200 (Welinder et al., 2010), Caltech101 (Fei-Fei et al., 2004), CIFAR-100 (Krizhevsky et al., 2009), and ImageNet (Deng et al., 2009). The following architectures of various sizes are pretrained on subsets of JFT-300M (Sun et al., 2017): big-transfer residual neural networks (BiT) (Kolesnikov et al., 2020), MLP mixers (MiX) (Tolstikhin et al., 2021), and vision transformers (ViT) (Dosovitskiy et al., 2020). As can be seen in Tables 1 and 4, BNSL yields extrapolations with the lowest RMSLE (Root Mean Squared Logarithmic Error) for 69.44% of tasks of any of the functional forms, while the next best functional form performs the best on only 13.89% of the tasks.

To view all plots of BNSL on each of these tasks, see figures 16, 17, 18, 19 in Appendix A.24. To view all plots of M1, M2, M3, and M4 on each of these tasks, see Appendix A.4 of Alabdulmohsin et al. (2022).

In Section A.13, we additionally show that BNSL yields accurate extrapolations of performance on large-scale downstream vision tasks when amount of compute used for (pre-)training is on the x-axis and compute is scaled in the manner that is Pareto optimal with respect to the performance evaluation metric on the y-axis (downstream accuracy in this case).

In Section A.14, we additionally show that BNSL yields accurate extrapolations of the scaling behavior of diffusion generative models of images when amount of compute used for (pre-)training is on the x-axis and compute is scaled in the manner that is Pareto optimal with respect to the performance evaluation metric on the y-axis (NLL and FID score in this case).

In Section A.15, we additionally show that BNSL yields accurate extrapolations of the scaling behavior of generative models of video.

In Section A.21, we show that BNSL accurately extrapolates the scaling behavior of the downstream performance of multimodal contrastive learning (i.e. non-generative unsupervised learning).

In Section A.16, we additionally show that BNSL yields accurate extrapolations of the scaling behavior when data is pruned Pareto optimally (such that each point along the x-axis uses the subset of the dataset that yields the best performance (y-axis value) for that dataset size (x-axis value)).

In Section A.17, we additionally show that BNSL yields accurate extrapolations when upstream performance is on the x-axis and downstream performance is on the y-axis.

In Section A.23, we additionally show that BNSL accurately extrapolates to scales that are an order of magnitude larger than the maximum (along the x-axis) of the points used for fitting.

Task	Model	M1 ↓	M2 ↓	M3 ↓	M4 ↓	BNSL ↓
Birds 200 10-shot	BiT/101/3	9.13e-2 ± 2.8e-3	9.13e-2 ± 2.8e-3	9.13e-2 ± 2.8e-3	2.95e-2 ± 1.3e-3	**1.76e-2 ± 1.1e-3**
Birds 200 10-shot	BiT/50/1	6.88e-2 ± 7.5e-4	6.88e-2 ± 7.5e-4	5.24e-2 ± 6.2e-4	2.66e-2 ± 5.3e-4	**1.19e-2 ± 3.5e-4**
Birds 200 10-shot	MiX/B/16	9.15e-2 ± 1.1e-3	9.15e-2 ± 1.1e-3	3.95e-2 ± 7.0e-4	4.62e-2 ± 8.2e-4	**3.04e-2 ± 6.9e-4**
Birds 200 10-shot	MiX/L/16	5.51e-2 ± 1.4e-3	5.51e-2 ± 1.4e-3	5.51e-2 ± 1.4e-3	5.15e-2 ± 1.7e-3	**1.85e-2 ± 8.9e-4**
Birds 200 10-shot	ViT/B/16	6.77e-2 ± 1.1e-3	6.77e-2 ± 1.1e-3	3.52e-2 ± 8.1e-4	**1.51e-2 ± 6.2e-4**	1.69e-2 ± 7.0e-4
Birds 200 10-shot	ViT/S/16	3.95e-2 ± 1.2e-3	3.95e-2 ± 1.2e-3	3.74e-2 ± 1.1e-3	1.85e-2 ± 7.9e-4	**1.09e-2 ± 6.1e-4**
Birds 200 25-shot	BiT/101/3	9.41e-2 ± 3.2e-3	9.41e-2 ± 3.2e-3	9.41e-2 ± 3.2e-3	6.38e-2 ± 2.0e-3	**1.55e-2 ± 1.3e-3**
Birds 200 25-shot	BiT/50/1	1.10e-1 ± 1.0e-3	7.29e-2 ± 8.0e-4	1.52e-2 ± 4.9e-4	1.97e-2 ± 5.6e-4	**1.33e-2 ± 4.4e-4**
Birds 200 25-shot	MiX/B/16	1.40e-1 ± 1.9e-3	1.40e-1 ± 1.9e-3	6.93e-2 ± 1.2e-3	2.11e-2 ± 6.9e-4	**1.64e-2 ± 6.6e-4**
Birds 200 25-shot	MiX/L/16	1.12e-1 ± 2.0e-3	1.12e-1 ± 2.0e-3	1.12e-1 ± 2.0e-3	5.44e-2 ± 1.8e-3	**2.08e-2 ± 1.1e-3**
Birds 200 25-shot	ViT/B/16	9.02e-2 ± 1.6e-3	9.02e-2 ± 1.6e-3	3.75e-2 ± 1.0e-3	**1.51e-2 ± 5.7e-4**	1.62e-2 ± 6.1e-4
Birds 200 25-shot	ViT/S/16	5.06e-2 ± 1.4e-3	5.06e-2 ± 1.4e-3	4.96e-2 ± 1.4e-3	4.02e-2 ± 1.2e-3	**1.03e-2 ± 6.6e-4**
Birds 200 5-shot	BiT/101/3	8.17e-2 ± 2.0e-3	8.17e-2 ± 2.0e-3	8.17e-2 ± 2.0e-3	3.38e-2 ± 1.3e-3	**1.81e-2 ± 8.2e-4**
Birds 200 5-shot	BiT/50/1	5.44e-2 ± 5.6e-4	5.44e-2 ± 5.6e-4	5.44e-2 ± 5.6e-4	2.59e-2 ± 5.4e-4	**1.34e-2 ± 3.7e-4**
Birds 200 5-shot	MiX/B/16	8.27e-2 ± 1.0e-3	8.27e-2 ± 1.0e-3	5.49e-2 ± 7.8e-4	2.14e-2 ± 5.3e-4	**1.39e-2 ± 4.1e-4**
Birds 200 5-shot	MiX/L/16	5.68e-2 ± 1.4e-3	5.68e-2 ± 1.4e-3	5.68e-2 ± 1.4e-3	3.20e-2 ± 9.7e-4	**1.85e-2 ± 6.4e-4**
Birds 200 5-shot	ViT/B/16	3.40e-2 ± 8.9e-4	3.40e-2 ± 8.9e-4	3.40e-2 ± 8.9e-4	1.65e-2 ± 6.7e-4	**1.36e-2 ± 5.8e-4**
Birds 200 5-shot	ViT/S/16	2.75e-2 ± 7.9e-4	2.75e-2 ± 7.9e-4	2.75e-2 ± 7.9e-4	1.20e-2 ± 5.2e-4	**7.39e-3 ± 4.5e-4**
CIFAR-100 10-shot	BiT/101/3	8.57e-2 ± 3.8e-3	8.57e-2 ± 3.8e-3	8.25e-2 ± 3.7e-3	4.77e-2 ± 3.0e-3	**2.58e-2 ± 2.3e-3**
CIFAR-100 10-shot	BiT/50/1	7.44e-2 ± 1.5e-3	1.24e-2 ± 5.8e-4	2.08e-2 ± 7.2e-4	**1.24e-2 ± 5.8e-4**	1.83e-2 ± 8.3e-4
CIFAR-100 10-shot	MiX/B/16	8.77e-2 ± 1.9e-3	8.77e-2 ± 1.9e-3	2.71e-2 ± 1.2e-3	**2.37e-2 ± 9.9e-4**	2.44e-2 ± 9.5e-4
CIFAR-100 10-shot	MiX/L/16	1.05e-1 ± 3.1e-3	1.05e-1 ± 3.1e-3	4.85e-2 ± 2.6e-3	4.97e-2 ± 1.6e-3	**4.75e-2 ± 2.6e-3**
CIFAR-100 10-shot	ViT/B/16	8.98e-2 ± 2.0e-3	8.98e-2 ± 2.0e-3	8.98e-2 ± 2.0e-3	4.98e-2 ± 1.7e-3	**3.71e-2 ± 1.4e-3**
CIFAR-100 10-shot	ViT/S/16	6.84e-2 ± 1.1e-3	**2.11e-2 ± 6.6e-4**	3.35e-2 ± 8.6e-4	2.54e-2 ± 7.5e-4	2.57e-2 ± 7.5e-4
CIFAR-100 25-shot	BiT/101/3	8.77e-2 ± 5.6e-3	8.77e-2 ± 5.6e-3	4.44e-2 ± 3.5e-3	3.40e-2 ± 2.7e-3	**2.88e-2 ± 3.0e-3**
CIFAR-100 25-shot	BiT/50/1	7.31e-2 ± 2.0e-3	2.35e-2 ± 1.5e-3	3.65e-2 ± 1.8e-3	2.35e-2 ± 1.5e-3	**1.89e-2 ± 1.1e-3**
CIFAR-100 25-shot	MiX/B/16	1.08e-1 ± 2.3e-3	4.75e-2 ± 1.6e-3	**2.10e-2 ± 9.4e-4**	2.24e-2 ± 9.9e-4	2.67e-2 ± 1.1e-3
CIFAR-100 25-shot	MiX/L/16	9.79e-2 ± 2.2e-3	9.79e-2 ± 2.2e-3	3.67e-2 ± 1.7e-3	**2.98e-2 ± 1.4e-3**	3.45e-2 ± 1.6e-3
CIFAR-100 25-shot	ViT/B/16	1.07e-1 ± 1.9e-3	1.07e-1 ± 1.9e-3	6.54e-2 ± 1.6e-3	4.80e-2 ± 1.4e-3	**3.02e-2 ± 4.5e-3**
CIFAR-100 25-shot	ViT/S/16	8.03e-2 ± 1.2e-3	2.19e-2 ± 7.4e-4	3.13e-2 ± 8.4e-4	2.27e-2 ± 7.1e-4	**2.14e-2 ± 6.9e-4**
CIFAR-100 5-shot	BiT/101/3	5.94e-2 ± 3.2e-3	5.94e-2 ± 3.2e-3	5.94e-2 ± 3.2e-3	**3.30e-2 ± 2.4e-3**	3.78e-2 ± 2.6e-3
CIFAR-100 5-shot	BiT/50/1	4.87e-2 ± 1.3e-3	4.87e-2 ± 1.3e-3	1.69e-2 ± 8.8e-4	1.87e-2 ± 8.9e-4	**1.45e-2 ± 8.7e-4**
CIFAR-100 5-shot	MiX/B/16	7.07e-2 ± 1.2e-3	7.07e-2 ± 1.2e-3	2.78e-2 ± 8.4e-4	1.76e-2 ± 6.6e-4	**1.70e-2 ± 6.3e-4**
CIFAR-100 5-shot	MiX/L/16	7.06e-2 ± 1.6e-3	7.06e-2 ± 1.6e-3	4.17e-2 ± 1.4e-3	3.32e-2 ± 1.2e-3	**2.77e-2 ± 1.0e-3**
CIFAR-100 5-shot	ViT/B/16	6.27e-2 ± 1.6e-3	6.27e-2 ± 1.6e-3	6.27e-2 ± 1.6e-3	4.30e-2 ± 1.3e-3	**2.82e-2 ± 1.0e-3**
CIFAR-100 5-shot	ViT/S/16	6.93e-2 ± 1.2e-3	**2.84e-2 ± 8.2e-4**	3.88e-2 ± 8.0e-4	3.16e-2 ± 7.5e-4	3.50e-2 ± 9.2e-3
Caltech101 10-shot	BiT/101/3	3.07e-1 ± 2.0e-2	3.07e-1 ± 2.0e-2	1.51e-1 ± 1.3e-2	1.00e-1 ± 1.1e-2	**4.75e-2 ± 8.1e-3**
Caltech101 10-shot	BiT/50/1	3.29e-1 ± 1.6e-2	7.68e-2 ± 5.0e-3	1.13e-1 ± 6.0e-3	6.01e-2 ± 4.4e-3	**1.77e-2 ± 2.5e-3**
Caltech101 10-shot	MiX/B/16	**1.35e-1 ± 1.4e-2**	1.35e-1 ± 1.4e-2	1.35e-1 ± 1.4e-2	1.92e-1 ± 1.6e-2	2.04e-1 ± 9.7e-3
Caltech101 10-shot	MiX/L/16	1.25e-1 ± 1.3e-2	1.25e-1 ± 1.3e-2	**1.25e-1 ± 1.3e-2**	1.30e-1 ± 1.2e-2	2.13e-1 ± 1.5e-2
Caltech101 10-shot	ViT/B/16	7.76e-2 ± 4.3e-3	7.76e-2 ± 4.3e-3	**3.11e-2 ± 3.0e-3**	5.75e-2 ± 4.4e-3	4.02e-2 ± 3.9e-3
Caltech101 10-shot	ViT/S/16	1.95e-1 ± 6.0e-3	3.41e-2 ± 2.9e-3	**2.40e-2 ± 2.0e-3**	3.41e-2 ± 2.9e-3	2.40e-2 ± 2.0e-3
Caltech101 25-shot	BiT/101/3	1.15e-1 ± 6.5e-3	1.15e-1 ± 6.5e-3	1.15e-1 ± 6.5e-3	1.15e-1 ± 6.5e-3	**9.86e-2 ± 8.0e-3**
Caltech101 25-shot	BiT/50/1	3.60e-1 ± 1.9e-2	8.80e-2 ± 5.5e-3	1.43e-1 ± 7.6e-3	4.76e-2 ± 3.6e-3	**1.55e-2 ± 1.6e-3**
Caltech101 25-shot	MiX/B/16	**8.28e-2 ± 1.2e-2**	8.28e-2 ± 1.2e-2	8.28e-2 ± 1.2e-2	1.65e-1 ± 1.7e-2	1.93e-1 ± 1.3e-2
Caltech101 25-shot	MiX/L/16	9.66e-2 ± 1.0e-2	9.66e-2 ± 1.0e-2	9.66e-2 ± 1.0e-2	**9.66e-2 ± 1.0e-2**	1.49e-1 ± 1.3e-2
Caltech101 25-shot	ViT/B/16	1.03e-1 ± 5.6e-3	**3.33e-2 ± 2.5e-3**	4.46e-2 ± 3.6e-3	3.33e-2 ± 2.5e-3	3.95e-2 ± 5.4e-3
Caltech101 25-shot	ViT/S/16	1.77e-1 ± 5.4e-3	3.79e-2 ± 3.1e-3	**2.80e-2 ± 1.8e-3**	3.79e-2 ± 3.1e-3	3.29e-2 ± 2.1e-3
Caltech101 5-shot	BiT/101/3	2.12e-1 ± 1.2e-2	2.12e-1 ± 1.2e-2	2.12e-1 ± 1.2e-2	1.65e-1 ± 9.4e-3	**1.87e-2 ± 4.3e-3**
Caltech101 5-shot	BiT/50/1	2.34e-1 ± 6.1e-3	4.13e-2 ± 2.1e-3	**1.61e-2 ± 1.3e-3**	4.69e-2 ± 2.1e-3	4.10e-2 ± 2.1e-3
Caltech101 5-shot	MiX/B/16	2.43e-1 ± 1.2e-2	2.43e-1 ± 1.2e-2	2.35e-1 ± 1.1e-2	7.28e-2 ± 4.3e-3	**1.92e-2 ± 1.9e-3**
Caltech101 5-shot	MiX/L/16	1.38e-1 ± 9.7e-3	1.38e-1 ± 9.7e-3	1.38e-1 ± 9.7e-3	**1.37e-1 ± 9.9e-3**	1.63e-1 ± 1.1e-2
Caltech101 5-shot	ViT/B/16	1.10e-1 ± 6.3e-3	1.10e-1 ± 6.3e-3	6.02e-2 ± 4.7e-3	6.81e-2 ± 4.8e-3	**3.87e-2 ± 3.4e-3**
Caltech101 5-shot	ViT/S/16	1.90e-1 ± 4.7e-3	3.82e-2 ± 2.6e-3	5.04e-2 ± 2.9e-3	3.82e-2 ± 2.6e-3	**2.78e-2 ± 1.8e-3**
ImageNet 10-shot	BiT/101/3	1.27e-1 ± 2.0e-3	1.27e-1 ± 2.0e-3	7.36e-2 ± 1.1e-3	3.06e-2 ± 7.0e-4	**6.65e-3 ± 3.8e-4**
ImageNet 10-shot	BiT/50/1	9.54e-2 ± 7.2e-4	9.54e-2 ± 7.2e-4	5.75e-3 ± 2.0e-4	1.86e-2 ± 2.8e-4	**3.84e-3 ± 1.5e-4**
ImageNet 10-shot	MiX/B/16	9.34e-2 ± 7.9e-4	9.34e-2 ± 7.9e-4	3.37e-2 ± 2.9e-4	2.32e-2 ± 3.0e-4	**4.22e-3 ± 1.5e-4**
ImageNet 10-shot	MiX/L/16	9.83e-2 ± 1.3e-3	9.83e-2 ± 1.3e-3	9.83e-2 ± 1.3e-3	**4.01e-3 ± 1.9e-4**	4.33e-3 ± 1.8e-4
ImageNet 10-shot	ViT/B/16	4.62e-2 ± 7.1e-4	4.62e-2 ± 7.1e-4	4.62e-2 ± 7.1e-4	1.44e-2 ± 3.0e-4	**5.70e-3 ± 2.0e-4**
ImageNet 10-shot	ViT/S/16	4.74e-2 ± 5.6e-4	4.74e-2 ± 5.6e-4	1.66e-2 ± 2.5e-4	7.18e-3 ± 2.0e-4	**3.71e-3 ± 1.4e-4**
ImageNet 25-shot	BiT/101/3	1.42e-1 ± 2.3e-3	1.42e-1 ± 2.3e-3	6.67e-2 ± 9.1e-4	3.31e-2 ± 8.7e-4	**4.76e-3 ± 2.8e-4**
ImageNet 25-shot	BiT/50/1	1.17e-1 ± 9.2e-4	1.17e-1 ± 9.2e-4	**4.06e-3 ± 1.7e-4**	1.84e-2 ± 2.6e-4	4.67e-3 ± 1.6e-4
ImageNet 25-shot	MiX/B/16	9.59e-2 ± 9.3e-4	9.59e-2 ± 9.3e-4	5.39e-2 ± 4.9e-4	2.04e-2 ± 3.1e-4	**4.17e-3 ± 1.7e-4**
ImageNet 25-shot	MiX/L/16	1.03e-1 ± 1.3e-3	1.03e-1 ± 1.3e-3	1.03e-1 ± 1.3e-3	**6.33e-3 ± 2.2e-4**	7.60e-3 ± 2.6e-4
ImageNet 25-shot	ViT/B/16	5.17e-2 ± 8.8e-4	5.17e-2 ± 8.8e-4	5.17e-2 ± 8.8e-4	1.52e-2 ± 3.8e-4	**4.96e-3 ± 2.0e-4**
ImageNet 25-shot	ViT/S/16	5.52e-2 ± 4.4e-4	4.12e-2 ± 3.4e-4	9.65e-3 ± 2.3e-4	7.78e-3 ± 2.1e-4	**6.11e-3 ± 2.4e-4**
ImageNet 5-shot	BiT/101/3	9.24e-2 ± 1.4e-3	9.24e-2 ± 1.4e-3	9.24e-2 ± 1.4e-3	2.09e-2 ± 7.9e-4	**8.05e-3 ± 5.0e-4**
ImageNet 5-shot	BiT/50/1	8.95e-2 ± 6.7e-4	8.95e-2 ± 6.7e-4	1.53e-2 ± 2.2e-4	1.11e-2 ± 2.3e-4	**7.94e-3 ± 2.1e-4**
ImageNet 5-shot	MiX/B/16	9.09e-2 ± 7.2e-4	9.09e-2 ± 7.2e-4	3.01e-2 ± 2.8e-4	1.95e-2 ± 2.7e-4	**6.49e-3 ± 2.2e-4**
ImageNet 5-shot	MiX/L/16	7.99e-2 ± 9.7e-4	7.99e-2 ± 9.7e-4	7.99e-2 ± 9.7e-4	9.92e-3 ± 4.5e-4	**5.68e-3 ± 2.4e-4**
ImageNet 5-shot	ViT/B/16	4.11e-2 ± 6.3e-4	4.11e-2 ± 6.3e-4	4.11e-2 ± 6.3e-4	1.55e-2 ± 2.8e-4	**1.29e-2 ± 2.7e-4**
ImageNet 5-shot	ViT/S/16	4.20e-2 ± 4.1e-4	4.20e-2 ± 4.1e-4	2.40e-2 ± 2.6e-4	8.02e-3 ± 1.9e-4	**4.72e-3 ± 1.6e-4**

Table 4: Extrapolation Results on scaling behavior of Downstream Vision Tasks. See Section A.9 for more details. Numbers for M1, M2, M3, and M4 obtained via correspondence with authors of Alabdulmohsin et al. (2022).

A.10 LANGUAGE

Using the scaling laws benchmark of Alabdulmohsin et al. (2022), we evaluate how well various functional forms extrapolate performance on language tasks as the training dataset size increases. In this large-scale language subset of the benchmark, the tasks that are evaluated are error rates on each of the various downstream tasks from the BIG-Bench (BB) (Srivastava et al., 2022) benchmark and upstream test cross-entropy of various models trained to do language modeling (LM) and neural machine translation (NMT). All LM and BB tasks use a decoder-only language model. As can be seen in Tables 1 and 5, BNSL yields extrapolations with the lowest RMSLE (Root Mean Squared Logarithmic Error) for 60% of tasks of any of the functional forms, while the next best functional form performs the best on only 25% of the tasks.

To view all plots of the BNSL on each of these tasks, see Figures 20, 21, 22 in Appendix A.24.

To view plots of M1, M2, M3, and M4 on these tasks, see Figure 8 of Alabdulmohsin et al. (2022).

In Section A.18, we additionally show that BNSL yields accurate extrapolations of performance on large-scale downstream language tasks when number of model parameters is on the x-axis.

In Section A.22, we additionally show that BNSL yields accurate extrapolations of performance on large-scale downstream audio (speech recognition) tasks.

Domain	Task	Model	M1 ↓	M2 ↓	M3 ↓	M4 ↓	BNSL ↓
BB	date understanding, 1-shot	2.62e+8 Param	3.19e-2 ± 9.6e-4	3.19e-2 ± 9.6e-4	**4.67e-3 ± 1.4e-4**	3.19e-2 ± 9.6e-4	1.81e-2 ± 3.9e-4
BB	date understanding, 2-shot	2.62e+8 Param	2.86e-2 ± 6.2e-4	2.86e-2 ± 6.2e-4	**4.83e-3 ± 4.1e-4**	2.86e-2 ± 6.2e-4	5.41e-3 ± 1.0e-3
BB	linguistic mappings, 1-shot	2.62e+8 Param	1.66e-2 ± 5.5e-4	1.62e-2 ± 5.4e-4	1.66e-2 ± 5.5e-4	1.33e-2 ± 3.8e-4	**1.13e-2 ± 2.2e-4**
BB	linguistic mappings, 2-shot	2.62e+8 Param	1.70e-2 ± 6.5e-4	1.70e-2 ± 6.5e-4	1.70e-2 ± 6.5e-4	1.06e-2 ± 5.1e-4	**9.51e-3 ± 5.1e-4**
BB	mult data wrangling, 1-shot	2.62e+8 Param	1.07e-2 ± 1.0e-3	1.07e-2 ± 1.0e-3	1.07e-2 ± 1.0e-3	6.66e-3 ± 7.3e-4	**6.39e-3 ± 4.6e-4**
BB	mult data wrangling, 2-shot	2.62e+8 Param	1.57e-2 ± 1.5e-3	1.57e-2 ± 1.5e-3	1.57e-2 ± 1.5e-3	5.79e-3 ± 7.0e-4	**2.67e-3 ± 2.7e-4**
BB	qa wikidata, 1-shot	2.62e+8 Param	**4.27e-3 ± 8.9e-4**	4.32e-3 ± 8.2e-4	4.27e-3 ± 8.9e-4	4.32e-3 ± 8.2e-4	4.68e-3 ± 7.3e-4
BB	qa wikidata, 2-shot	2.62e+8 Param	**4.39e-3 ± 7.0e-4**	4.66e-3 ± 6.4e-4	4.39e-3 ± 7.0e-4	9.02e-3 ± 6.9e-4	8.05e-3 ± 7.3e-4
BB	unit conversion, 1-shot	2.62e+8 Param	8.30e-3 ± 4.4e-4	8.30e-3 ± 4.4e-4	**1.48e-3 ± 2.7e-4**	4.79e-3 ± 3.4e-4	5.73e-2 ± 4.6e-3
BB	unit conversion, 2-shot	2.62e+8 Param	1.07e-2 ± 4.4e-4	1.07e-2 ± 4.4e-4	**7.50e-3 ± 5.5e-4**	7.55e-3 ± 5.1e-4	7.74e-2 ± 5.7e-3
LM	upstream test cross-entropy	1.07e+9 Param	1.71e-2 ± 6.0e-4	1.66e-3 ± 5.1e-5	4.50e-3 ± 5.9e-5	1.28e-3 ± 3.9e-5	**9.71e-4 ± 3.2e-5**
LM	upstream test cross-entropy	4.53e+8 Param	1.65e-2 ± 6.6e-4	7.41e-4 ± 9.8e-5	6.58e-4 ± 6.6e-5	7.41e-4 ± 9.8e-5	**5.86e-4 ± 7.7e-5**
LM	upstream test cross-entropy	2.62e+8 Param	1.55e-2 ± 7.2e-4	9.20e-4 ± 9.7e-5	3.97e-3 ± 1.3e-4	9.20e-4 ± 9.7e-5	**7.90e-4 ± 5.1e-5**
LM	upstream test cross-entropy	1.34e+8 Param	1.43e-2 ± 4.8e-4	1.46e-3 ± 6.8e-5	**6.46e-4 ± 5.1e-5**	1.46e-3 ± 6.8e-5	9.01e-4 ± 5.5e-5
LM	upstream test cross-entropy	1.68e+7 Param	6.37e-3 ± 9.4e-5	**3.03e-4 ± 1.2e-5**	1.56e-3 ± 3.5e-5	3.03e-4 ± 1.2e-5	4.34e-4 ± 1.8e-5
NMT	upstream test cross-entropy	28 Enc, 6 Dec	1.71e-1 ± 0	5.64e-2 ± 0	3.37e-2 ± 0	1.81e-2 ± 0	**1.69e-2 ± 0**
NMT	upstream test cross-entropy	6 Enc, 28 Dec	2.34e-1 ± 0	5.27e-2 ± 0	1.65e-2 ± 0	4.44e-2 ± 0	**1.56e-2 ± 0**
NMT	upstream test cross-entropy	6 Enc, 6 Dec	2.62e-1 ± 0	3.84e-2 ± 0	8.92e-2 ± 0	2.05e-2 ± 0	**1.37e-3 ± 0**
NMT	upstream test cross-entropy	Dec-only, LM	2.52e-1 ± 0	1.03e-2 ± 0	3.28e-2 ± 0	8.43e-3 ± 0	**7.33e-3 ± 0**
NMT	upstream test cross-entropy	Transformer-Enc, LSTM-Dec	1.90e-1 ± 0	1.26e-2 ± 0	6.32e-2 ± 0	1.26e-2 ± 0	**8.30e-3 ± 0**

Table 5: Extrapolation Results on scaling behavior of Language Tasks. See Section A.10 for more details. Numbers for M1, M2, M3, and M4 were obtained via correspondence with authors of Alabdulmohsin et al. (2022). BB stands for BIG-Bench (Srivastava et al., 2022). NMT stands for Neural Machine Translation. LM stands for Language Modeling.

A.11 REINFORCEMENT LEARNING

We show that BNSL accurately models and extrapolates the scaling behaviors of various multi-agent and single-agent reinforcement learning algorithms trained in various environments. In the top left plot and top right plot and bottom left plot of Figure 3, BNSL accurately models and extrapolates the scaling behavior of the AlphaZero algorithm trained to play the game Connect Four from Figure 4 and Figure 5 and Figure 3 respectively of Neumann & Gros (2022); the x-axes respectively are compute (FLOPs) used for training, training dataset size (states), and number of model parameters. In Figure 3 bottom right, BNSL accurately models and extrapolates the scaling behavior of the Proximal Policy Optimization (PPO) algorithm (Schulman et al., 2017) trained to play the Procgen (Cobbe et al., 2020) game called Heist.

In Section A.19, we find BNSL accurately extrapolates the scaling behavior of a pretrained language model finetuned (i.e. aligned) via Reinforcement Learning from Human Feedback (RLHF) to be helpful from Figure 1 of Bai et al. (2022).

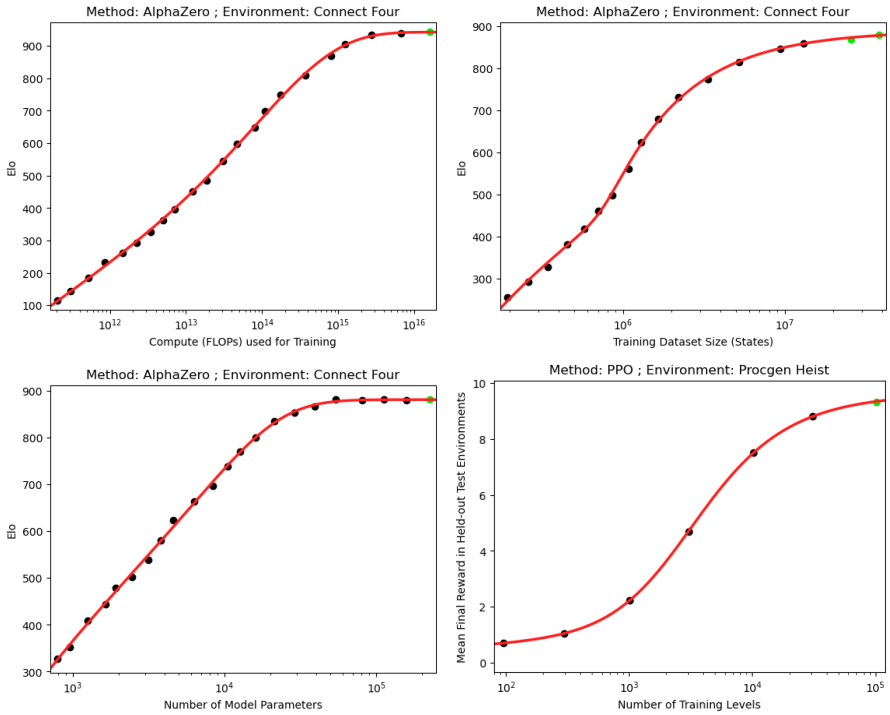

Figure 3: Extrapolation of BNSL on Reinforcement Learning Scaling Experimental Data. Experimental data of the top left plot and top right plot and bottom left plot is from Figure 4 and Figure 5 and Figure 3 respectively of Neumann & Gros (2022). Experimental Data of the bottom right plot is from Figure 2 of Cobbe et al. (2020). Top left plot is the compute-optimal Pareto frontier. See Section A.11 for more details.

A.12 NON-MONOTONIC SCALING

We show that BNSL accurately models and extrapolates non-monotonic scaling behaviors that are exhibited by Transformers (Vaswani et al. (2017)) in double descent (Nakkiran et al., 2021) in Figure 4. Various other functional forms are mathematically incapable of expressing non-monotonic behaviors (as shown in Section A.8).

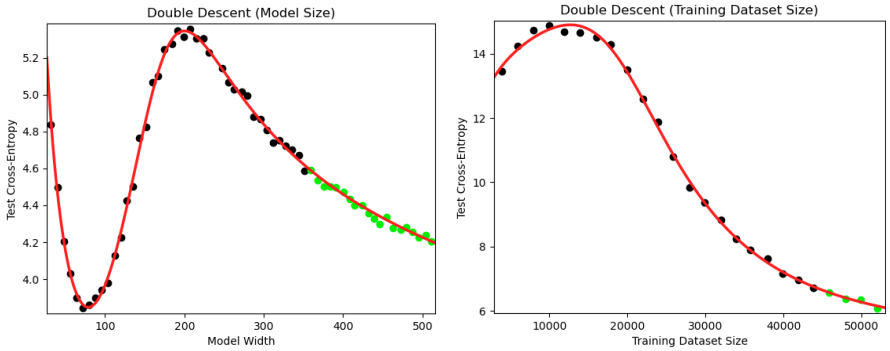

Figure 4: Extrapolation of BNSL on Double Descent. Both plots are of transformers trained to do neural machine translation via minimizing cross-entropy. Experimental data of left figure is obtained from Figure 8 top of Nakkiran et al. (2021); "Model Width" on the x-axis refers to embedding dimension d_{model} of the transformer. Experimental data of the right figure is obtained from Figure 11b of Nakkiran et al. (2021). The plot on the left contains two breaks of a BNSL fit to the black points. See Section A.12 for more details.

A.13 EXTRAPOLATION RESULTS FOR DOWNSTREAM VISION TASKS WHEN TRAINING RUNS ARE SCALED TO BE COMPUTE-OPTIMAL.

Task	Model	M3 ↓	BNSL ↓
ImageNet 10-Shot	ViT	1.91e-2 ± 6.48e-3	**9.79e-3 ± 4.70e-3**
ImageNet Finetune	ViT	1.14e-2 ± 2.42e-3	**9.37e-3 ± 2.60e-3**

Table 6: Extrapolation Results for Downstream Vision Tasks when training runs are scaled using the compute-optimal scaling (i.e. Pareto frontier) with respect to downstream performance. Experimental data obtained from Figure 2 of Zhai et al. (2021). See Section A.13 for more details.

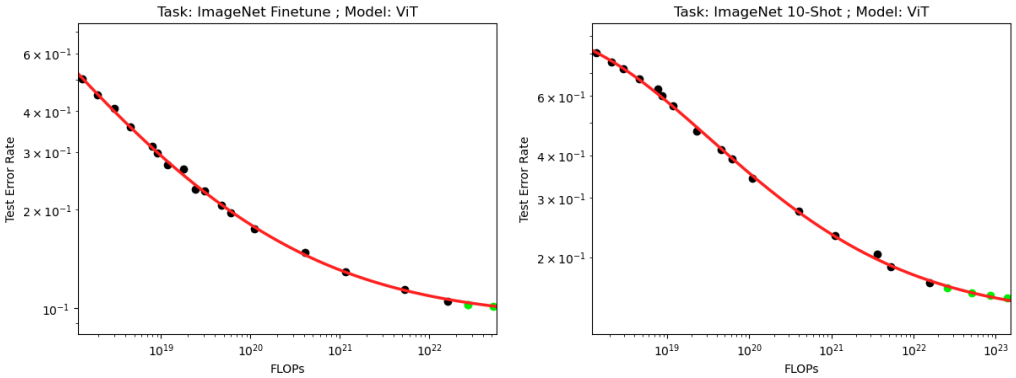

Figure 5: Extrapolation Results of BNSL for Downstream Vision Tasks when training runs are scaled to be compute-optimal. Experimental data obtained from Figure 2 of Zhai et al. (2021). See Section A.13 for more details.

In Figure 5 via fitting BNSL, we additionally obtain accurate extrapolations of scaling behavior of large-scale downstream vision tasks when compute (FLOPs) used for (pre-)training is on the x-axis and compute is scaled in the manner that is Pareto optimal with respect to the performance evaluation metric (downstream accuracy in this case). The experimental scaling data was obtained from Figure 2 of Zhai et al. (2021), and a result in Table 6 we compare extrapolation of BNSL to the extrapolation of M3 (which was proposed in Zhai et al. (2021)); we find that BNSL that yields extrapolations of scaling behavior that are more accurate on these tasks.

A.14 EXTRAPOLATION RESULTS FOR DIFFUSION GENERATIVE MODELS OF IMAGES

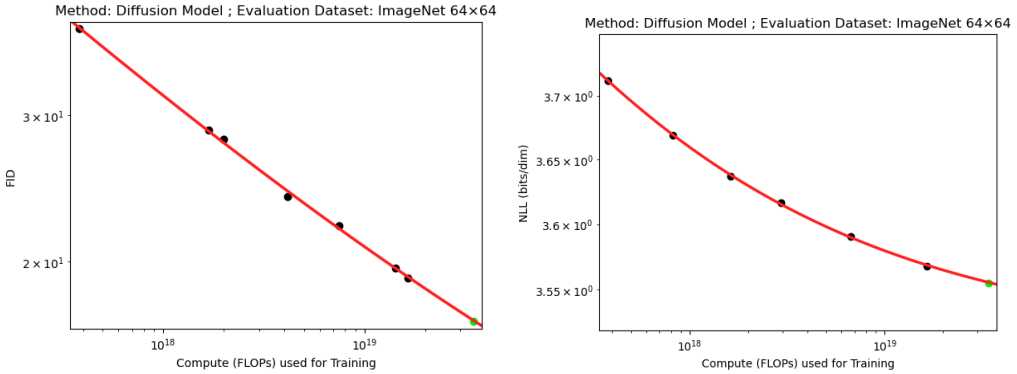

Figure 6: Extrapolation Results of BNSL for scaling behavior of Diffusion Generative Models of Images. Frechet Inception Distance (FID) score is on the y-axis in the left plot. Negative log-likelihood (NLL) is the y-axis in the right plot. For both plots, compute used for training is on the x-axis and Imagenet 64x64 is the evaluation dataset. Experimental data of scaling behavior obtained from Figure 10 of Nichol & Dhariwal (2021). See Section A.14 for more details.

In Figure 6, we show that BNSL accurately extrapolates the scaling behavior of Diffusion Generative Models of Images from Figure 10 of Nichol & Dhariwal (2021) when Negative Log-likelihood (NLL) or Frechet Inception Distance (FID) score is on the y-axis and compute used for training is on the x-axis; compute is scaled in the manner that is Pareto optimal with respect to the performance evaluation metric on the y-axis.

A.15 EXTRAPOLATION RESULTS FOR GENERATIVE MODELS OF VIDEO

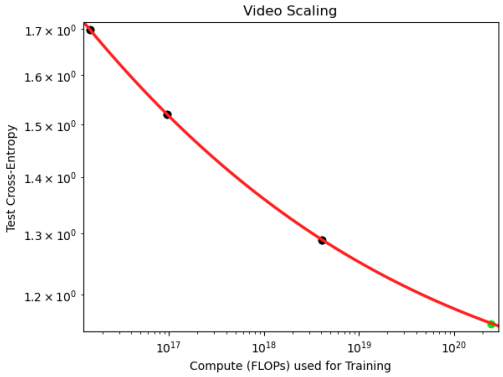

Figure 7: Extrapolation Results of BNSL for scaling behavior of Generative Models of Video. Upstream Test Cross-Entropy is on the y-axis. Videos scraped from the web are the evaluation dataset. During training, compute (used for training autoregressive transformer) on the x-axis is scaled in the manner that is Pareto optimal with respect to the performance evaluation metric on the y-axis. Experimental data of scaling behavior obtained from top right plot of Figure 5 of Henighan et al. (2020). See Section A.15 for more details.

In Figure 7, we show that BNSL accurately extrapolates the scaling behavior of generative models of video. Each frame is downsampled to a pixel resolution of 64x64; each frame is then tokenized via a pretrained 16x16 VQVAE (Van Den Oord et al., 2017) to obtain 256 tokens per frame. 16 consecutive frames are then input to an autoregressive transformer as a length 4096 (16x16x16) sequence. The dataset is 100 hours of videos scraped from the web. See section 2 of Henighan et al. (2020) for more details.

A.16 EXTRAPOLATION RESULTS WHEN DATA IS PRUNED PARETO OPTIMALLY

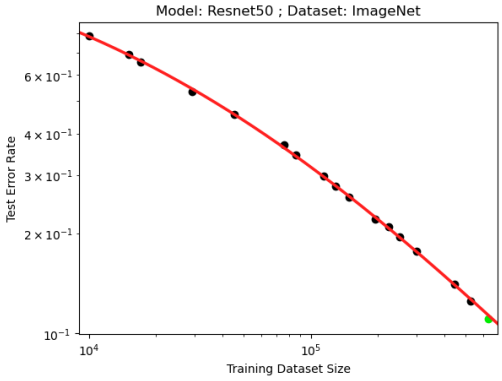

Figure 8: Extrapolation Results of BNSL for scaling behavior when data is pruned Pareto optimally (such that each point along the x-axis uses the subset of the dataset that yields the best performance (y-axis value) for that dataset size (x-axis value)). Experimental data of scaling behavior obtained from Figure 3D of Sorscher et al. (2022). See Section A.16 for more details.

In Figure 8, we show that BNSL accurately extrapolates the scaling behavior when data is pruned Pareto optimally (such that each point along the x-axis uses the subset of the dataset that yields the best performance (y-axis value) for that dataset size (x-axis value)) from Figure 3D of Sorscher et al. (2022).

A.17 EXTRAPOLATION RESULTS WHEN UPSTREAM PERFORMANCE IS ON THE X-AXIS

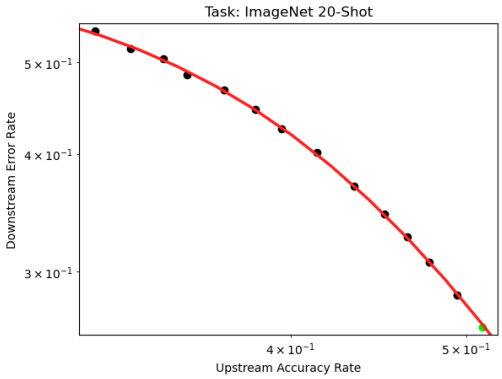

Figure 9: Extrapolation Results of BNSL for scaling behavior when Upstream Performance is on the x-axis and Downstream Performance is on the y-axis. Experimental data of scaling behavior obtained from Figure 5 of Abnar et al. (2021). The upstream task is supervised pretraining of ViT (Dosovitskiy et al., 2020) on subsets of JFT-300M (Sun et al., 2017). The Downstream Task is 20-shot ImageNet classification. See Section A.17 for more details.

In Figure 9, we show that BNSL accurately extrapolates the scaling behavior when upstream performance is on the x-axis and downstream performance is on the y-axis. The upstream task is supervised pretraining of ViT (Dosovitskiy et al., 2020) on subsets of JFT-300M (Sun et al., 2017). The downstream task is 20-shot ImageNet classification. The experimental data of this scaling behavior is obtained from Figure 5 of Abnar et al. (2021).

A.18 EXTRAPOLATION RESULTS FOR DOWNSTREAM LANGUAGE TASKS WHEN NUMBER OF MODEL PARAMETERS IS ON THE X-AXIS.

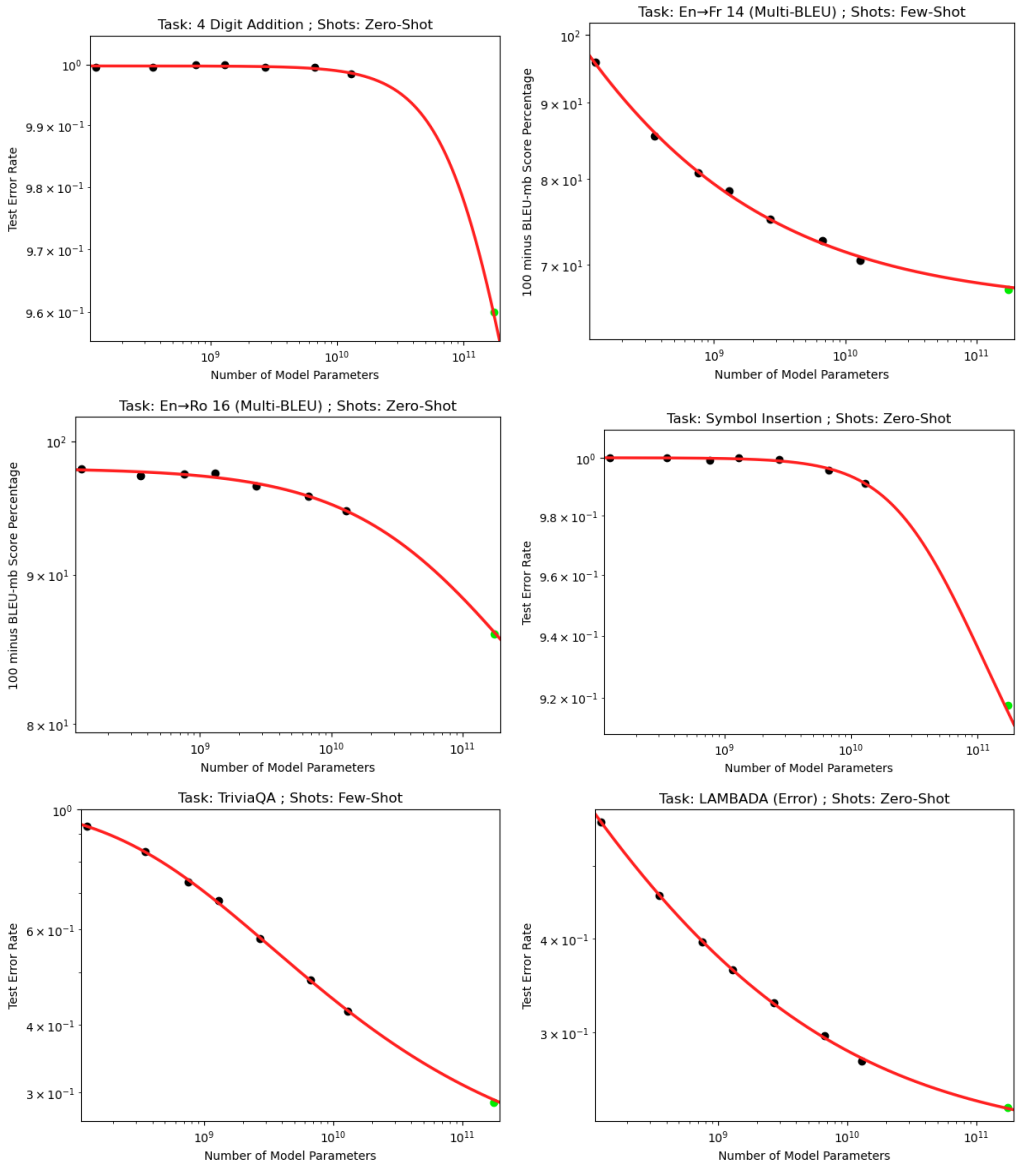

Figure 10: Extrapolation Results for Downstream Language Tasks when Number of Model Parameters is on the x-axis. Experimental data obtained from Table H.1 of the GPT-3 arXiv paper (Brown et al., 2020). See Section A.18 for more details.

We find in general for each of every modality that the variance between seeds is higher when number of model parameters is on x-axis (as opposed to e.g. training dataset size on the x-axis). Table H.1 of the GPT-3 arXiv paper (Brown et al., 2020) release includes results for 8 numbers of model parameters. In Figure 10, we include examples of when 8 numbers of model parameters (7 for fitting, and largest held-out to evaluate extrapolation) are sufficient for obtaining accurate downstream extrapolation due to variance between seeds being low enough. For many other downstream tasks with number of model parameters on the x-axis, the variance between seeds is much higher such that a number considerably larger than 7 points along the curve is needed to obtain an accurate extrapolation.

A.19 EXTRAPOLATION RESULTS FOR AI ALIGNMENT VIA RLHF

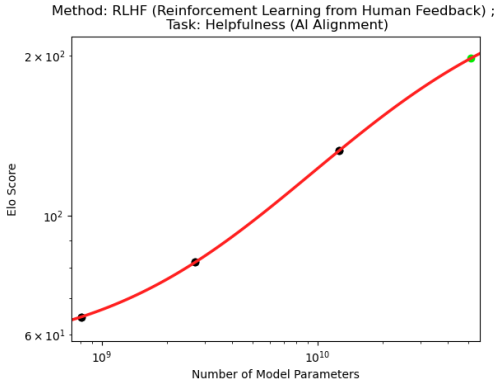

Figure 11: Extrapolation Results for Downstream AI Alignment when Number of Model Parameters is on the x-axis. Experimental data obtained from the Static HH RLHF results from Figure 1 of Bai et al. (2022). See Section A.19 for more details.

In Figure 11, we find BNSL accurately extrapolates the scaling behavior of a pretrained language model finetuned (i.e. aligned) via Reinforcement Learning from Human Feedback (RLHF) to be helpful from Figure 1 of Bai et al. (2022). The y-axis is Elo score based on crowdworker preferences. The x-axis is the number of model parameters that the language model contains.

A.20 EXTRAPOLATION RESULTS FOR ROBOTICS

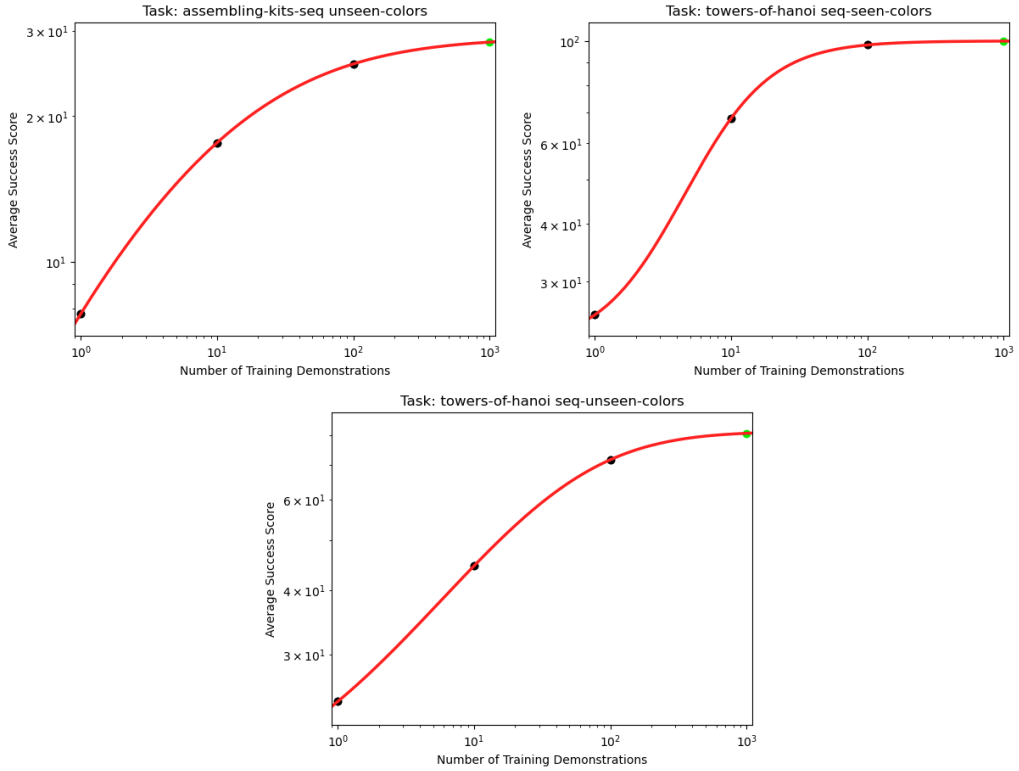

Figure 12: Extrapolation Results for Robotic control. Experimental data obtained from the transporter (Zeng et al., 2021) model results from Table 1 of Shridhar et al. (2021). X-axis is number training demonstrations. Y-axis is task success score (mean percentage) obtained via 100 evaluations. See Section A.20 for more details.

In Figure 12, we find BNSL accurately extrapolates the scaling behavior of a transporter (Zeng et al., 2021) model trained via imitation learning to do robotic control tasks.

A.21 EXTRAPOLATION RESULTS FOR DOWNSTREAM PERFORMANCE OF MULTIMODAL CONTRASTIVE LEARNING (I.E. NON-GENERATIVE UNSUPERVISED LEARNING)

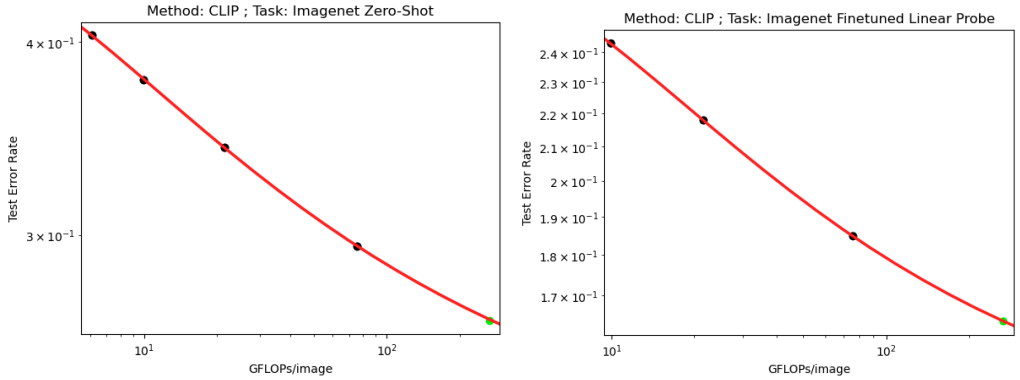

Figure 13: Extrapolation Results of BNSL for Downstream Performance of Multimodal Contrastive Learning (i.e. Non-Generative Unsupervised Learning). Experimental data of scaling behavior obtained from Table 10 and Table 11 in arXiv version of Radford et al. (2021). The upstream task is "Contrastive Image Language Pretraining" (a.k.a. CLIP) of ResNets on a training dataset consisting of hundreds of millions of image-text pairs. The x-axis is GFLOPs/image (GigaFLOPs/image) of the forward-pass of model. The Downstream Task is ImageNet classification (i.e. the y-axis of plot). The y-axis of left plot is Zero-Shot Downstream. The y-axis of right plot is performance of model with finetuned linear probe on it. See Section A.21 for more details.

In Figure 14, we show that BNSL accurately extrapolates the scaling behavior of the Downstream Performance of Multimodal Contrastive Learning (i.e. Non-Generative Unsupervised Learning).

A.22 EXTRAPOLATION RESULTS FOR DOWNSTREAM PERFORMANCE ON AUDIO TASKS

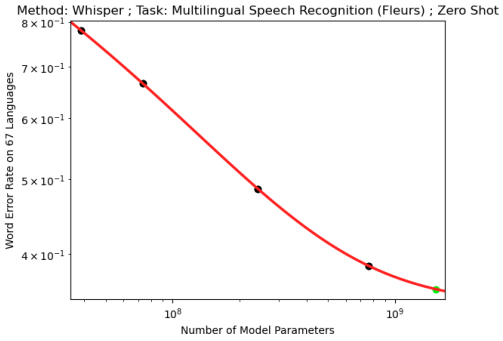

Figure 14: Extrapolation Results of BNSL for Downstream Audio Tasks when Number of Model Parameters is on the x-axis. Experimental data obtained from the second plot of Figure 6 of Whisper paper (Radford et al., 2022). The downstream task in the plot is downstream zero shot multilingual speech recognition performance on the FLEURS dataset of "Whisper" speech recognition model pretrained on a dataset of 681,070 hours of audio. See Section A.22 for more details.

In Figure 14, we show that BNSL accurately extrapolates the scaling behavior of the Downstream Performance on Audio Tasks.

A.23 EXTRAPOLATION TO SCALES THAT ARE AN ORDER OF MAGNITUDE LARGER THAN THE MAXIMUM (ALONG THE X-AXIS) OF THE POINTS USED FOR FITTING

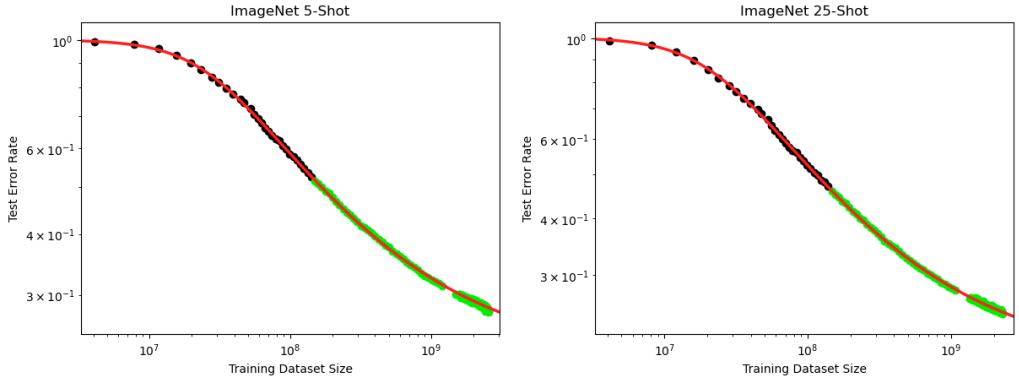

Figure 15: Extrapolation Results of BNSL to Scales that are an Order of Magnitude larger than the maximum (along the x-axis) of the points used for fitting. Experimental data of scaling behavior obtained from Figure 5 of Abnar et al. (2021). The upstream task is supervised pretraining of MLP mixers (MiX) (Tolstikhin et al., 2021) on subsets (i.e. the x-axis of plot) of JFT-300M (Sun et al., 2017). The Downstream Task is n-shot ImageNet classification (i.e. the y-axis of plot). See Section A.23 for more details.

In Figure 15, we show that BNSL accurately extrapolates to scales that are an order of magnitude larger than the maximum (along the x-axis) of the points used for fitting. The upstream task is supervised pretraining of MLP mixers (MiX) (Tolstikhin et al., 2021) on subsets (i.e. the x-axis of plot) of JFT-300M (Sun et al., 2017). The downstream task is n-shot ImageNet classification (i.e. the y-axis of plot). The experimental data of this scaling behavior is obtained from Alabdulmohsin et al. (2022).

A.24 PLOTS OF BNSL EXTRAPOLATIONS ON SCALING LAWS BENCHMARK OF ALABDULMOHSIN ET AL. (2022)

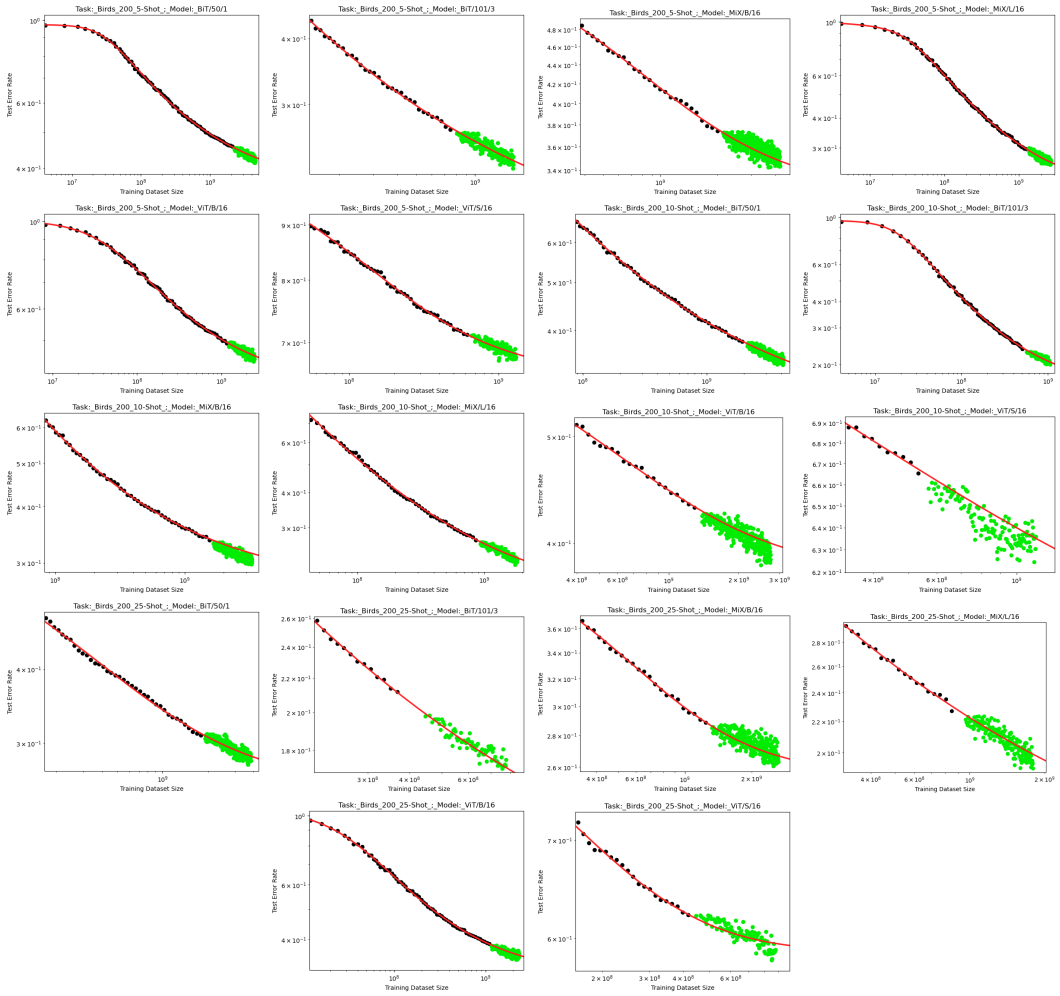

Figure 16: Birds 200

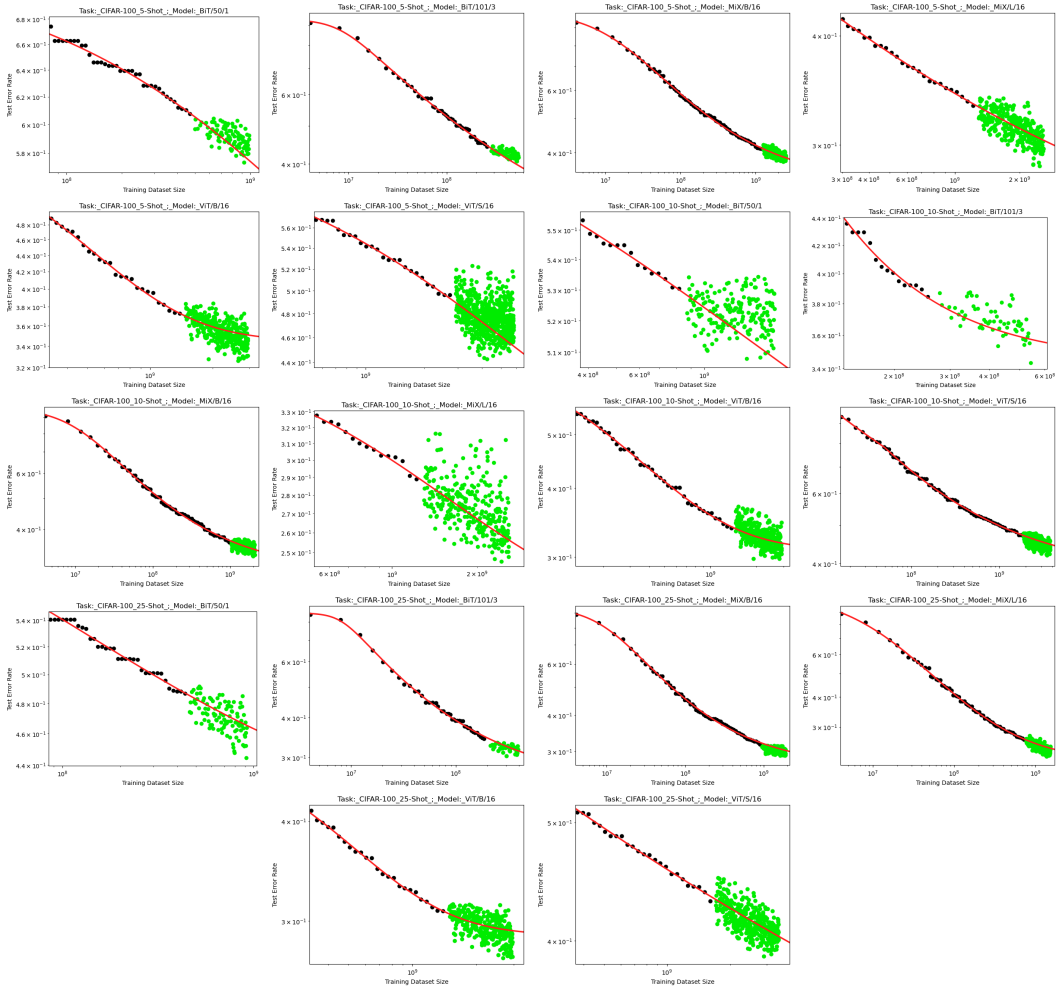

Figure 17: CIFAR-100

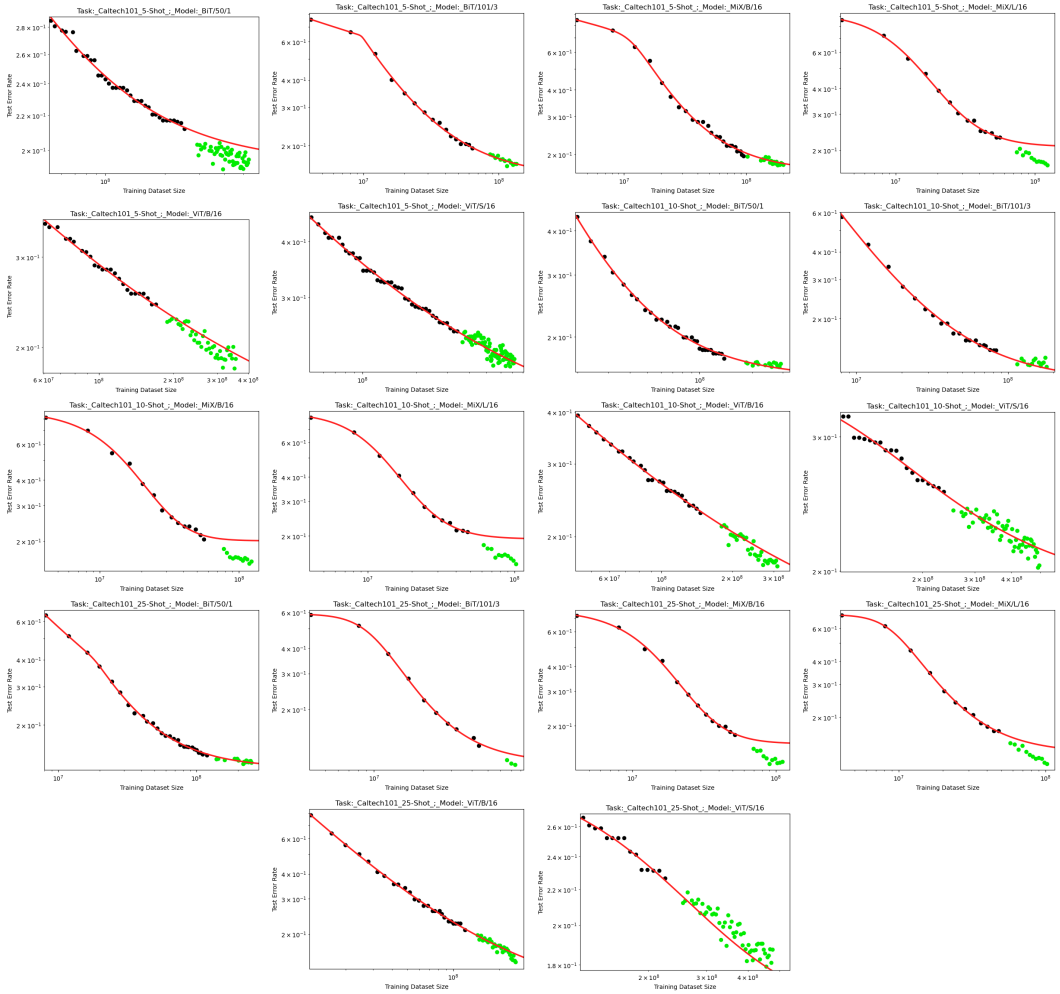

Figure 18: Caltech101. From eyeballing, we think the subset of Caltech101 with unsatisfactory extrapolations has unsatisfactory extrapolations due to the maximum (along the x-axis) of the black point used for fitting being near or before a break; this is accentuated by not having enough points for fitting for the SciPy fitter to be able to determine whether the break is an actual break or just noisy deviation. See Section 4 for more details on this explanation.

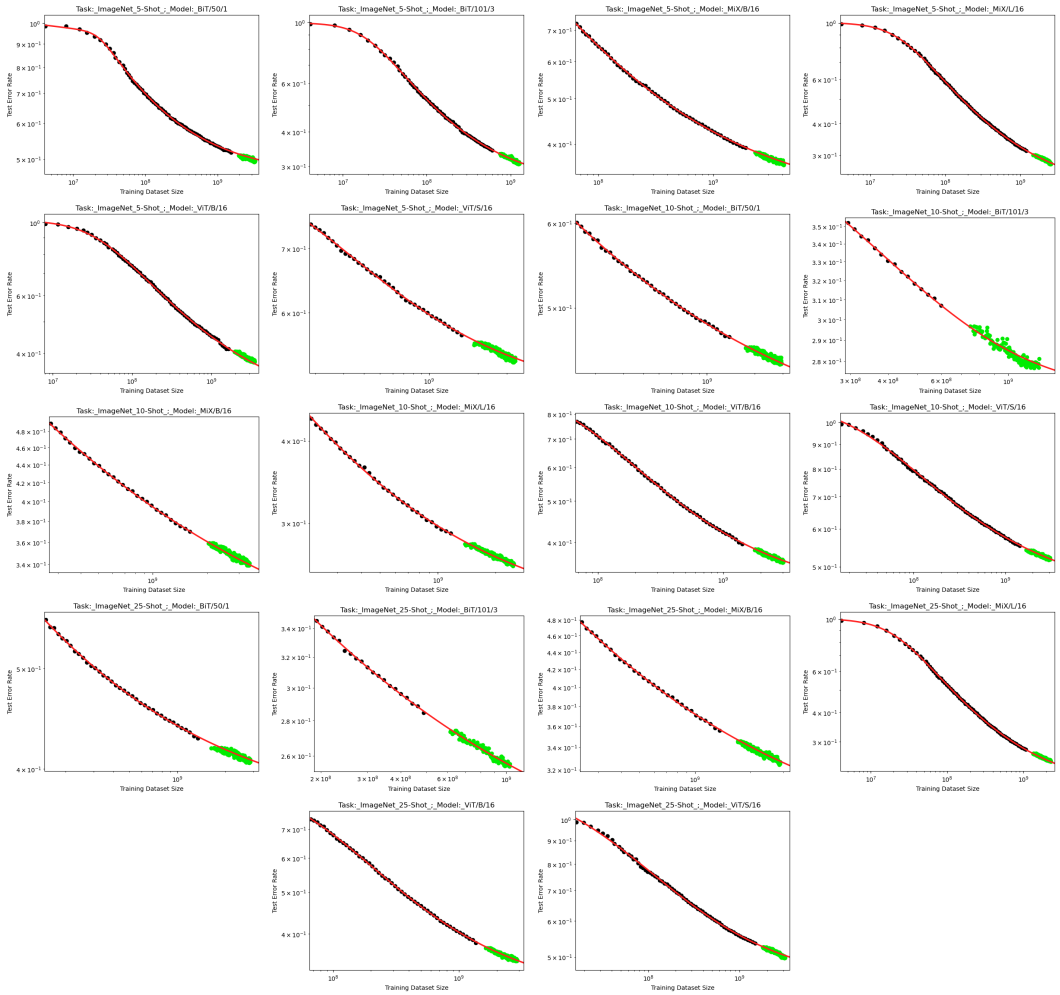

Figure 19: ImageNet

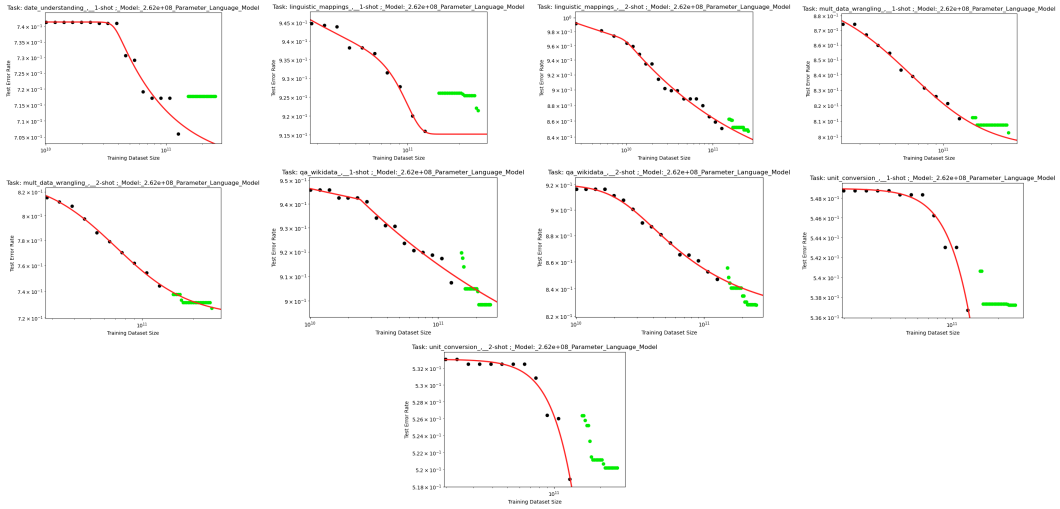

Figure 20: BIG-Bench (BB). From eyeballing, we think the subset of BIG-Bench with unsatisfactory extrapolations has unsatisfactory extrapolations due to the maximum (along the x-axis) of the black point used for fitting being near or before a break; this is accentuated by not having enough points for fitting for the SciPy fitter to be able to determine whether the break is an actual break or just noisy deviation. See Section 4 for more details on this explanation.

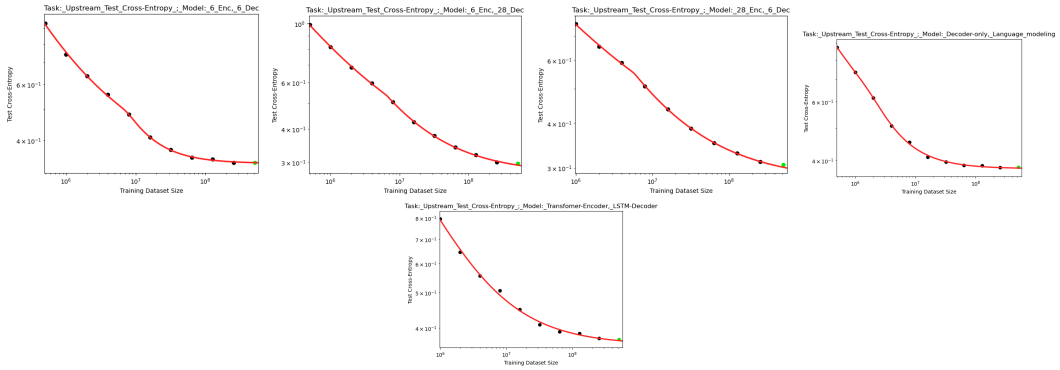

Figure 21: Neural Machine Translation (NMT)

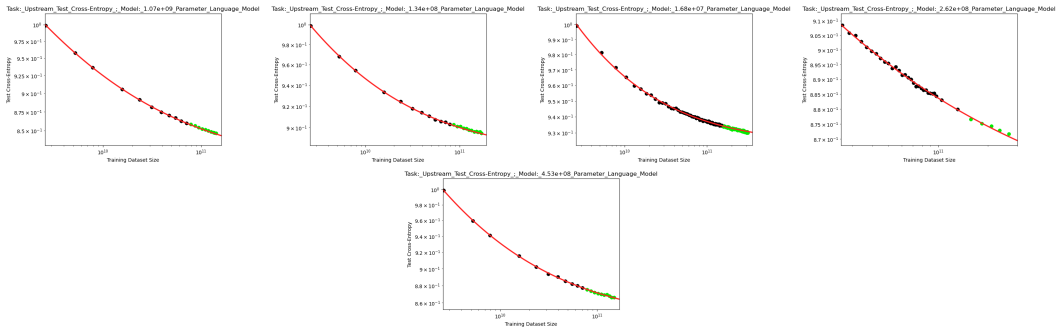

Figure 22: Language Modeling (LM)